

Ice Nucleating Particles Variability Across a Megacity

Sebastián Mendoza-Téllez¹, Karla Valdés², David Ramírez², Jan Alexis Cedillo³, Olivia Rivera-Hernández⁴, Fernanda Córdoba¹, Harry Alvarez⁵, Javier Miranda⁶, Irma Rosas¹, Graciela B. Raga¹, Emma Negrete¹, Leticia Martínez¹, Eva Salinas¹, and Luis A. Ladino^{1,*}

¹Institute for Atmospheric Sciences and Climate Change, Universidad Nacional Autónoma de México, Mexico City, Mexico

²División de Ciencias Biológicas y de la Salud, Universidad Autónoma Metropolitana – Xochimilco, Mexico City, Mexico

³Escuela Nacional de Ciencias Biológicas, Instituto Politécnico Nacional, Mexico City, Mexico

⁴Dirección de Monitoreo de Calidad del Aire, Secretaría del Medio Ambiente, Ciudad de México, Mexico

⁵Facultad de Ciencias, Universidad Nacional Autónoma de México, Mexico City, Mexico

⁶Instituto de Física, Universidad Nacional Autónoma de México, Mexico City, Mexico

*Corresponding author: Luis A. Ladino (luis.ladino@atmosfera.unam.mx)

Abstract

Megacities are a great source of urban aerosol particles, which can impact cloud formation and the local hydrological cycle. However, the aerosol-cloud interaction in megacities, especially in their different micro-climates, is poorly understood. In the present study, the physicochemical and biological properties of urban aerosol particles, along with their **ice nucleating particle (ice nucleation abilities INP) concentration** via immersion freezing and as a function of particle size (~~4.00.56~~ μm to $10 \mu\text{m}$), were simultaneously characterized at two sites across the Mexico City Metropolitan Area (MCMA). We found ~~apparent~~ differences in the chemical composition, criteria pollutants ($\text{PM}_{2.5}$, O_3 , CO , NO_x , and SO_2), and biological content between ~~northern and southern~~ sites in the MCMA, separated by 16 km. The collected urban MCMA aerosol particles were found to act as ~~ice nucleating particles (INPs)~~, with average concentrations ranging between $(0.04 \pm 0.04) \text{ L}^{-1}$ (at -15°C) and ~~(24.93 ± 187)~~ L^{-1} (at 30°C). Although the measured INP concentrations are were similar across the MCMA in both sites, the southern samples showed a higher INP concentration for larger aerosol particles (i.e., particles between $5.6\text{-}10 \mu\text{m}$) than northern samples. The southern MCMA samples were found to be more efficient INPs, and their ice nucleation abilities correlated positively with $\text{PM}_{2.5}$, potassium, and sulfur. On the other hand, the ice nucleation abilities of the measured urban particles at both sites did not correlate with their size nor the presence of biological particles. Overall, although the urban aerosol's physicochemical properties, and biological content, composition, and ~~s and, their~~ its sources were found to, and their role in cloud

41 ~~formation~~ INP concentration at both sites were found to be differ at both sites, it did not
42 strongly impacted the INP concentrations, with the exception of the largest measured particles.
43 ~~. Therefore, the present results demonstrated the presence of two different distinct micro-~~
44 ~~climates within the MCMA and~~ an unknown contribution from large particles to INP
45 concentrations in the southern microclimate. ~~This h~~ This h ~~Highlights~~ sings the importance ~~to~~
46 ~~consider~~ of considering that aerosol-cloud interactions within a megacity may vary ~~widely,~~
47 especially when assessing the role of INPs in cloud formation ~~the development of extreme~~
48 precipitation events.

49

50 **1. Introduction**

51 Mexico City and its Metropolitan Area (MCMA) is one of the top megacities worldwide with
52 a population of 21 million inhabitants (Población, 2025). In the 1980s, the MCMA was reported
53 as the most polluted city on Earth (Molina and Molina, 2004); however, since the 1990s, air
54 quality has improved significantly (Lezama and Vargas, 2000). Even so, due to its size and the
55 diverse anthropogenic activities, the MCMA atmospheric processes are complex and far from
56 being completely understood (Molina et al., 2010). Nowadays, poor air quality is one of the
57 major threats for the MCMA inhabitants' health (Riojas-Rodríguez et al., 2014). The impact of
58 the high annual release of particulate matter (PM) (in the order of gigagrams, Gg) on the local
59 climate remains poorly quantified (Castro Romero et al., 2024).

60

61 Several studies have provided substantial ~~information to improve our understanding of~~ insights
62 into the physicochemical properties of PM ~~along within~~ the MCMA (Aldape et al., 1991;
63 Edgerton et al., 1999; Doran et al., 2007; Querol et al., 2008). For example, Vega et al. (2004)
64 characterized the PM_{2.5} composition of the MCMA, showing that the sulfate (SO₄²⁻),
65 ammonium (NH₄⁺), and total carbon (elemental carbon + organic carbon) average
66 concentrations are higher in the north of the city compared to the southern part (higher by 1.16
67 $\mu\text{g m}^{-3}$ (18.1 %), 0.8 $\mu\text{g m}^{-3}$ (23.6 %), and 18.49 $\mu\text{g m}^{-3}$ (51.1 %), respectively). This agrees
68 with the data reported by the 2006 MILAGRO (Megacity Initiative: Local And Global Research
69 Observations) project, where a complete evaluation of the regional and global impacts of
70 Mexico's City atmospheric emissions was assessed (Molina et al., 2010).

71

72 Several studies found that organic matter has a huge impact on the MCMA's PM_{2.5}
73 composition. Amador-Muñoz et al. (2011) reported a carbon preference index (CPI) larger than
74 1 on the southwest of the MCMA, suggesting that this part of the city contains more biogenic

75 sources (Amador-Muñoz et al., 2013). Ladino et al. (2018) and Hernández-López et al. (2023)
76 reported clear differences in polycyclic aromatic hydrocarbons (PAHs) between the north and
77 south of the MCMA, with the highest concentrations reported in the northern part of the city.
78 Gasoline-fueled vehicles are likely responsible for local PAHs emissions and could reinforce
79 the presence of urban micro-climates with independent local atmospheric processes, inside one
80 megacity theory, which remarks how local emissions at one megacity's location can promote
81 important local atmospheric processes (Molina and Molina, 2004).

82
83
84

85 A microclimate can be referred as a relative small-scale area with a distinctive climate over it
86 as a whole (Met Office Factsheet 14). Thanks to its large area, and the clear variability of land
87 use (e.g., industrial, rural, residential, commerce, and ecological preservation), the northern and
88 southern MCMA present significant differences in temperature (heat islands), rainfall, wind
89 patterns, humidity, aerosol and gas emissions, indicating the presence of a clear microclimate
90 differentiation (Met Office Factsheet 14; Molina and Molina, 2004; Amador-Muñoz et al.,
91 2013; Castro Romero et al., 2024). ~~A microclimate can be referred as a relative small-scale area~~
92 ~~with a distinctive climate over itthe area as a whole (Met Office Factsheet 14). Thanks to its~~
93 ~~large space area, and the clear variability of useresidential, commerce, and ecological~~
94 ~~preservation, MCMA present differences in temperature (heat islands), rainfall, wind patterns,~~
95 ~~humidity, aerosol and gas emissions, the presence of a clear microclimate differentiation (Met~~
96 ~~Office Factsheet 14; Molina and Molina, 2004; Amador Muñoz et al., 2013; Castro Romero et~~
97 ~~al., 2024).~~

98

99 Although the studies above highlight the clear differences in the sources and physicochemical
100 properties of PM in different parts of the MCMA, studies that include simultaneous
101 measurements at two or more sites are scarce. This is of high importance to understand the
102 micro-climates along the MCMA and their relationship with local precipitation events. E.g.,
103 (Zhu et al., (2024) ~~evaluated~~ followed precipitation events across China, finding that
104 precipitation event characteristics could differ across climatic zones. ~~In~~ additionally, (Li et
105 al., (2019) showed that atmospheric circulation changes driven by warming modulated the
106 intensification of extreme precipitation events across North America.

107

108 [Meteorological data and models indicate a predominance of northerly, southerly, southwesterly,](#)
109 [and northeasterly wind events in MCMA, with frequencies of 20 %, 16 %, 15 %, and 13 %, respectively](#)
110 [\(Celada-Murillo et al., 2013\). In addition, typically wind events with speeds](#)
111 [ranging from 0.25 to 1.50 m /s⁻¹ appear mainly during the early morning, while other wind](#)
112 [events with larger speeds \(i.e., ranging from 1.5 to 5.50 m /s\) appear mainly during the](#)
113 [afternoon and night](#) (Celada-Murillo et al., 2013; Salcido et al., 2015). [On the other hand,](#)
114 [meteorological conditions in some defined area, as the presence of atmospheric stable](#)
115 [conditions, or the well-known large-scale atmospheric circulation could help understanding the](#)
116 [real perturbations of urban aerosols on cloud formation and precipitation events](#) (Trofimov et
117 al., 2022).

118
119 Given that most of the precipitation over the tropics comes from ice-containing clouds
120 (Mülmenstädt et al., 2015) and that aerosol particles acting as ice nucleating particles (INPs)
121 are key in mixed-phase cloud (MPC) formation (Rogers and Yau, 1996; Houze, 2014; Kanji et
122 al., 2017), [information on](#) the interplay between aerosol particles and cloud formation in big
123 cities such as the MCMA is urgently needed, especially because extreme precipitation events
124 are predicted to increase with time (Tabari, 2020; Gimeno et al., 2022), causing huge
125 economical and societal impacts in densely populated cities. [Aerosol particles have the potential](#)
126 [to influence the development of deep convective clouds those of which are typically associated](#)
127 [with extreme rainfall events](#) (Burrows et al., 2022). [Efficient INPs can promote specific](#)
128 [processes as the seeder-feeder mechanism](#) (Ohneiser et al., 2025) [triggering primary ice particle](#)
129 [formation as well as ice multiplication, increasing the ice water content in MPC](#) (Purdy et al.,
130 2005). [These ice particles can grow at expenses of the surrounding water droplets, via the](#)
131 [Wegner-Bergeron-Findeisen process, enhancing precipitation rates](#) (Heymsfield et al., 2020;
132 Ohneiser et al., 2025). [Toll et al. \(2024\) showed that the presence of anthropogenic particles](#)
133 [hot spots can modify cloud microphysics, leading to cloud glaciation and precipitation events](#)
134 [under stratiform non-convective clouds.](#)

135
136 The impact of urban particles on ice formation in MPCs is well documented (e.g., Hasenkopf
137 et al., 2016; Pereira et al., 2021; Chen et al., 2024). [For example, Numerous studies such as that](#)
138 [of Zhao et al. \(2019\),](#) reported that the presence of urban aerosol particles affects the
139 microphysical properties of clouds under moderate convective conditions, decreasing ice
140 crystal number concentration (ICNC) and thus increasing the ice particle effective radius (R_{ei}).
141 Chen et al. (2024) found that urban super-micron traffic-influenced road dust and construction-

142 related dust particles were the primary source of INPs (heat-resistant INPs) at temperatures
143 below -15 °C in Beijing, China. Nevertheless, given that urban aerosol particles are a complex
144 multicomponent mixture (i.e., biological, dust, black carbon, and biomass burning (BB)
145 particles, among others), they may contain components with contrasting ice nucleation abilities.
146 Although urban centers clearly experience high aerosol concentrations, INP concentrations in
147 megacities do not necessarily increase during heavily polluted periods (e.g., Bi et al., 2019;
148 Cabrera-Segoviano et al., 2022; Chen et al., 2024).

149
150 The role of urban particles emitted in the MCMA in ice-cloud formation has been previously
151 evaluated (Knopf et al., 2010; Pereira et al., 2021; Rodríguez-Gómez, 2021; Cabrera-Segoviano
152 et al., 2022; Melchum et al., 2023). The first ice nucleation study in the MCMA was conducted
153 by Knopf et al. (2010) as part of the MILAGRO project. The authors reported that the particles
154 in the northern part of the City are dominated by organics, and can efficiently act as INP under
155 cirrus [and MPC](#) conditions, i.e., relative humidity with respect to ice (RH_{ice}) of ~ 10522 % to
156 15028 % and temperatures of 20510 K to 25530 K.

157
158 Regarding MPC, Pereira et al. (2021) found that the ubiquitous anthropogenic emissions did
159 not have a significant impact on the INP concentrations, with samples collected in rural and
160 urban sites, both in the south of the MCMA. Cabrera-Segoviano et al. (2022) reported an inter-
161 annual variability of INP concentrations (a one order of magnitude difference at temperatures
162 higher than -20 °C) at southern MCMA between 2018 and 2019, a fact that can be related to the
163 variability in aerosol emissions like re-suspended dust. Rodríguez-Gómez (2021) reported
164 higher INP concentrations in the planetary boundary layer compared to the free troposphere on
165 samples collected in southern MCMA during the BB season, similar to previous studies (Prenni
166 et al., 2012; Jahn et al., 2020; Jahl et al., 2021). Finally, Melchum et al. (2023) evaluated the
167 INP abilities of different airborne microorganisms from tropical places such as MCMA and other
168 sites along Mexico. The authors found that out of the 64 tested microorganisms, only the
169 *Cupriavidus pauculus* ([B](#)proteobacteria) and the *Phaeocystis* sp. (marine phytoplankton) can
170 be relevant to MPC formation (with onset freezing temperatures, T_0 of -11.8 °C and -16.0 °C,
171 respectively).

172
173 Although PM and INPs have been previously characterized in the MCMA, simultaneous INP
174 measurements at more than one site have never been reported. Therefore, there is [a poor](#)
175 understanding of [the aerosol-cloud interactions show urban aerosol particles could influence](#)

176 ~~cloud formation within across the~~ different ~~micro-climates of the~~ MCMA's microclimates. To
177 fill this gap in knowledge, the present study reports the simultaneous characterization (physical,
178 chemical, and biological) of PM_{2.5} as well as the ~~ir-ice-nucleating-abilities~~ INP concentration in
179 ~~a~~ northern and ~~a~~ southern sites within the MCMA. To the best of our knowledge, this is the first
180 time that such comprehensive evaluation of the aerosol-cloud interactions is performed in this
181 megacity.

182

183 **2. Methods**

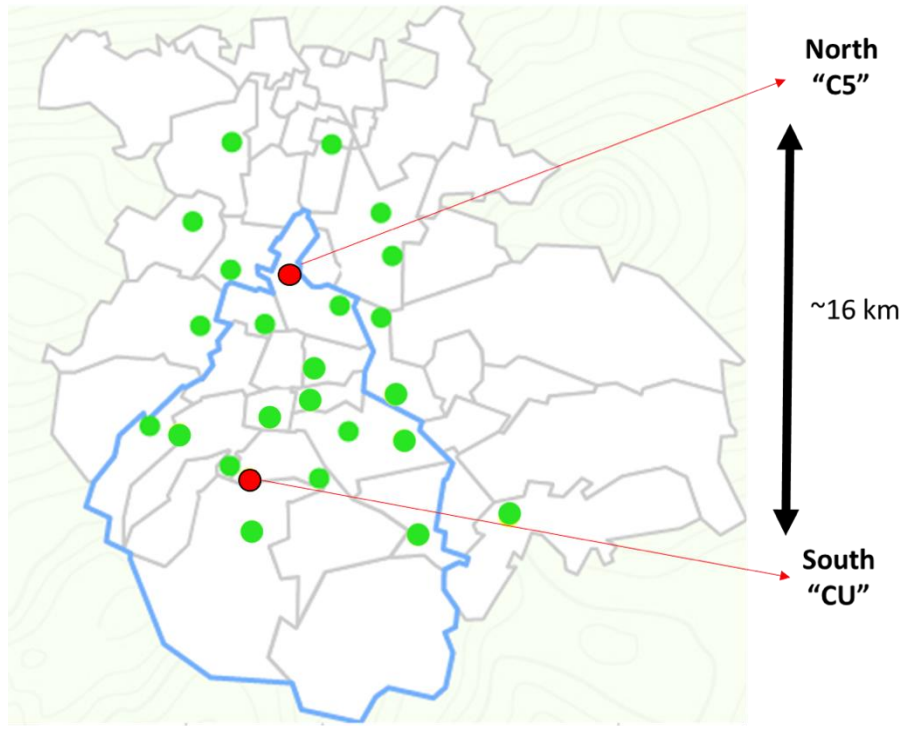
184 **2.1 Sampling location**

185 Mexico City is a tropical city located at 2240 m a.s.l. (Población, 2025), with a particular
186 topography that influences the accumulation of air pollutants (Molina and Molina, 2004). With
187 a sub-humid climate, the city presents an average annual temperature (between 1950 and 2013)
188 of 15 to 18 °C (Behzadi et al., 2020). The MCMA experiences three different seasons such as
189 cold-dry: October-February, warm-dry: March-May, and wet season: June-October. The mean
190 annual precipitation within 1950–2013 for Mexico City was reported to vary between 357 mm
191 year⁻¹ and 1298 mm year⁻¹ (Jáuregui, 2000; Molina et al., 2009; Behzadi et al., 2020; Cabrera-
192 Segoviano et al., 2022).

193

194 A short-term field campaign was carried out simultaneously at the north and south of the
195 MCMA during the dry-warm season, i.e., between May 12th and May 20th, 2022. Both
196 sampling sites are located within Mexico City (Fig. 1), and they are ~16 km away from each
197 other.

198



199

200 Figure 1. Location of the MCMA showing Mexico City (blue contour) as well as northern and
 201 southern sampling sites (red circles). The green and yellow circles represent the Mexico City
 202 atmospheric monitoring stations. Modified from <https://aire.cdmx.gob.mx/>

203

204 Sampling at the southern site (CU, 19.3262° N 99.1761° W) took place on the roof of the
 205 Institute for Atmospheric Sciences and Climate Change building (approx. 15 m a.g.l.), on the
 206 main campus of the Universidad Nacional Autónoma de México (UNAM). Traffic is the
 207 primary source of anthropogenic pollution at this site. However, an ecological reserve (237 ha)
 208 is located within the main UNAM campus, with the vegetation being dry and brown and
 209 susceptible to forest fires during the sampling period. It can provide biological material to the
 210 atmosphere through the native and introduced species of plants, animals, and microorganisms
 211 that live in it (Melchum et al., 2023).

212

213 On the other hand, the sampling at the northern site (C5, 19.483781° N 99.147312° W) took
 214 place on the roof of the Environmental Analysis Laboratory (C5) building (approx. 5 m a.g.l.)
 215 of the Mexico City Atmospheric Monitoring System (<http://www.aire.cdmx.gob.mx/>). The C5
 216 sampling site is subject to a wide range of anthropogenic sources, as it is located in the city's
 217 popularly known “industrial area.” Traffic, industrial, and other anthropogenic emissions
 218 contribute to high PM atmospheric concentrations at this sampling site (Castro Romero et al.,
 219 2024).

220
221
222
223
224
225
226
227
228
229
230
231
232
233
234
235
236
237
238
239

Meteorological (T, RH, wind direction, wind speed, solar radiation, and precipitation) and criteria pollutants (PM_{2.5}, O₃, CO, NO_x, and SO₂~~CO, O₃, SO₂, NO_x, and PM_{2.5}~~) data were recorded on both sites during the sampling campaign (Tables S1 and S2, and Figs. S1 and S2). The campaign dates, total sampling times and volumes are shown in ~~and sampling hours for the INP abilities are shown in~~ Table 1. Additionally, the ~~The~~ ionic composition and ~~and~~ elemental composition and ~~culturable microorganisms' identification was/were~~ obtained using ion chromatography and ~~and~~ X-ray fluorescence, respectively, on the 24-hour collected samples. Culturable microorganisms ~~were~~ obtained ~~and through~~ different microbiological analysis described in section 2.2.5, on 5 min collected samples. All sampling was performed ~~on the 24-hour samples collected~~ on May 12th, May 13th, May 16th, May 17th, May 18th, May 19th and May 20th, 2022.

Table 1. Sampling campaign description: d ~~D~~ates, times, and ~~total sampling times, and sampling volume are shown~~ for the three sampling methods: MiniVol (2.5 μm cut-off) for chemical analysis, MOUDI (0.56 to 10 μm cut-off, see section 2.2.6) for INP analysis, and BioStage (10 μm cut-off) for biological analysis ~~samples used to obtain the INP concentrations~~. Note that the sampling times were ~~was~~ the same at both sites.

SAMPLING CAMPAIGN								
Date (month- day- year)	MiniVol ¹ (chemical analysis)		MOUDI ² (INP analysis)				BioStage ³ (biological analysis)	
	Total sampling time (h)	Sampling volume (m ³)	Initial sampling time (local time, h)	Final sampling time (local time, h)	Total sampling time (h)	Sampling volume (m ³)	Total sampling time (h)	Sampling volume (m ³)
<u>05-12-22</u>	<u>24</u>	<u>7.2</u>	-	-	-	-	<u>0.08</u>	<u>0.1</u>
<u>05-13-22</u>	<u>24</u>	<u>7.2</u>	-	-	-	-	<u>0.08</u>	<u>0.1</u>
<u>05-14-22</u>	<u>24</u>	<u>7.2</u>	-	-	-	-	<u>0.08</u>	<u>0.1</u>
<u>05-15-22</u>	<u>24</u>	<u>7.2</u>	-	-	-	-	<u>0.08</u>	<u>0.1</u>
<u>05-16-22</u>	<u>24</u>	<u>7.2</u>	<u>8:37</u>	<u>12:58</u>	<u>4:21</u>	<u>7.8</u>	<u>0.08</u>	<u>0.1</u>
<u>05-17-22</u>	<u>24</u>	<u>7.2</u>	<u>8:20</u>	<u>12:20</u>	<u>4:00</u>	<u>7.2</u>	<u>0.08</u>	<u>0.1</u>
<u>05-18-22</u>	<u>24</u>	<u>7.2</u>	<u>8:04</u>	<u>12:06</u>	<u>4:02</u>	<u>7.3</u>	<u>0.08</u>	<u>0.1</u>
<u>05-19-22</u>	<u>24</u>	<u>7.2</u>	<u>8:44</u>	<u>12:56</u>	<u>4:12</u>	<u>7.6</u>	<u>0.08</u>	<u>0.1</u>
<u>05-20-22</u>	<u>24</u>	<u>7.2</u>	<u>8:43</u>	<u>12:50</u>	<u>4:07</u>	<u>7.4</u>	<u>0.08</u>	<u>0.1</u>

Flow rates: ¹5 L /min⁻¹, ²30 L /min⁻¹, ³28.3 L /min⁻¹

240
241
242
243
244
245
246
247
248
249
250
251
252
253
254
255
256
257
258
259
260
261
262
263
264
265
266
267
268
269
270
271
272
273

2.2 Sampling and instrumentation

The simultaneous sampling was performed using, per site, a MiniVol TAS (Tactical Air Sampler; Airmetrics) with a 2.5 μm cut-size inlet ~~that~~ operated at 5 L min^{-1} , an eight stage micro-orifice uniform deposit impactor (MOUDI 100R; MSP) operated at a 30 L min^{-1} flow rate to separate particles as a function of their aerodynamic diameter (cut sizes of 0.18 μm , 0.32 μm , 0.56 μm , 1.0 μm , 1.8 μm , 3.2 μm , 5.6 μm and 10 μm), and a single-stage BioStage Quick Take 30 cascade impactor for viable particles (SKC Inc. USA) operated at a 28.3 L min^{-1} flow rate. The MOUDI samples, used to evaluate the INP concentrations, were collected one time a day from May 16th to May 20th, 2022, with the sampling times shown in Table 1 (more details are provided in section 2.2.6). The MiniVol samples were collected daily for 24 h on May 12th, May 13th, May 16th, May 17th, May 18th, May 19th and May 20th, 2022, on 47 mm Teflon filters (Pall Science), ~~which and~~ were used for the ionic and elemental composition analysis. The BioStage impactor samples with a 10 μm cut-size inlet ~~consisted of and were,~~ used for culturable bacteria and fungi identification. They, were collected once a day (at 10:00 am for 5 mins) on the same dates as the MiniVol samples (more details are described in section 2.2.5). The general description of the sampling campaign is shown in Table 1.~~The BioStage impactor was used to collect bacteria and fungi identification (more details are described in section 2.2.5), and the MOUDI samples were used to evaluate the sample's ice nucleating abilities (more details are provided in section 2.2.6).~~

2.2.1 Meteorological data

Meteorological variables such as temperature, relative humidity, wind direction, wind speed, and solar radiation were obtained from the meteorological stations (Campbell ~~and DavisScientific~~) of the Red Universitaria de Observatorios Atmosféricos (RUOA) and the Programa de Estaciones Meteorológicas del Bachillerato Universitario (PEMBU) placed in CU and C5, respectively. Also, back trajectories of the air masses arriving in both sampling sites were obtained using the Hybrid Single-Particle Lagrangian Integrated Trajectory (HYSPLIT) model from the National Oceanic and Atmospheric Administration (NOAA) for 72 h at 250 ~~and 500~~ m a.g.l (Draxler, 2010).

2.2.2 Criteria pollutants

274 The concentrations of O₃, CO, NO_x, and SO₂, were measured with the Teledyne (Sandiego,
275 CA) ultraviolet photometry API Model 400E non-dispersive infrared analyzer, API model
276 300E, and API model 200E, respectively. The PM_{2.5} was measured with a Thermo Scientific
277 (Franklin, MA) tapered element oscillating microbalance (TEOM) Model 1400A ambient
278 particulate monitor at a flow rate of 3 L min⁻¹.

279

280 **2.2.3 PM_{2.5} ionic composition**

281 The ionic composition was obtained using a Dionex ICS-1500 ion chromatography (IC) at the
282 Laboratorio de Aerosoles Atmosféricos of the Institute for Atmospheric Sciences and Climate
283 Change, UNAM. For PM_{2.5} aerosol sample extraction, the [MiniVol sample 47-mm Teflon](#) filters
284 [\(i.e., 47 mm Teflon filters\)](#) were submerged in 10 mL of deionized water, sonicated for one
285 hour (using an ultrasonic bath at a temperature below 27 °C), and shaken at 350 rpm for six
286 hours (Sartorius CPA225D).

287

288 Anion analysis was performed using a Dionex IonPac AS23 column (4 × 250 mm) and a
289 carbonate solution (Na₂CO₃ 4.5 mM – NaHCO₃ 0.8 mM) as the mobile phase at a flow rate of
290 1 mL min⁻¹. Three anions [\(i.e., NO₃⁻, SO₄⁻², and Cl⁻\)](#) were measured using the described setup
291 ~~(NO₃⁻, SO₄⁻², and Cl⁻)~~. Cation analysis was performed using a Dionex IonPac CS12A column
292 (4 mm × 250 mm) and a methanesulfonic acid (CH₄O₃S 20 mM) with a flow rate of 1 mL min⁻¹
293 as a mobile phase. Five cations [\(i.e., Na⁺, K⁺, NH₄⁺, and Ca²⁺\)](#) were measured using the
294 described setup ~~(Na⁺, K⁺, NH₄⁺, and Ca²⁺)~~. The limits of quantification (LOQ) and
295 determination (LOD) were calculated using the linear regression of standards calibration. More
296 details about IC setup and similar methods can be found in Castro Romero et al. (2024).

297

298 **2.2.4 PM_{2.5} X-ray fluorescence**

299 The elemental composition analysis was performed at the Laboratorio de Aerosoles, Instituto
300 de Física, UNAM following Espinosa et al. (2012). An X-ray fluorescence spectrometer with
301 an Oxford Instruments (Scotts Valley, CA, USA) tube with Rh anode and an Amptek X-
302 123SDD spectrometer (Bedford, MA, USA) was used to obtain the elemental composition of
303 all ~~the~~ [MiniVol](#) particle samples. The instrument was operated at 50 kV and a current of 750
304 μA, irradiating for 900 s per spectrum. More details of instrument calibration can be found at
305 ~~(Espinosa et al., (2012))~~. The chemical composition was quantified using the methodology
306 reported by Espinosa et al. (2010). The percentage fraction for each element was determined

307 by using the relationship between the analyzed element concentration and the total mass
308 concentration.

309

310 **2.2.5 Airborne culturable microorganisms' collection and identification**

311 For the microorganism's identification (bacteria and fungi), petri dishes (100 mm × 10 mm)
312 with three different media were used to impact and, collect particles of 10 µm or less in size,
313 and grow the microorganisms using the BioStage impactor: trypto-casein soy agar (TSA, BD,
314 Bioxon) supplemented with 100 mg L⁻¹ of cycloheximide (Sigma-Aldrich) (to prevent growth
315 fungal propagules) for mesophilic cultivable bacteria (MCB), Reasoner's 2A (R2A, Condalab)
316 for slow-growing species of MCB, and malt extract agar (MEA, BD Bioxon) for cultivable
317 fungal propagules. The sampling time on the BioStage impactor was set to 5 min.

318

319 The concentrations of cultivable bacteria were reported as Colony Forming Units per m³ of air
320 (CFU m⁻³). The following procedure was applied as described in Melchum et al. (2023). The
321 TSA, R2A, and MEA were cultured at 357 °C, 35 °C, and 25 °C, respectively. After 48 h (for
322 TSA bacteria) and 72 h (for R2A bacteria and fungi), the CFU were quantified, and the Petri
323 dishes were sealed with parafilm and stored at 4 °C for further analysis. Representative bacterial
324 colonies were randomly selected and purified by several reseedings in TSA. Gram staining was
325 performed to classify the bacteria as Gram-positive or Gram-negative by microscopic
326 observation (100×) of the preparations. Isolated bacteria confirmation of identity was
327 performed by mass spectroscopy, using the Microflex MALDI-214-TOF MS® (Bruker
328 Daltonics, Bremen, Germany). The identification of fungal species was carried out at the genus
329 level using taxonomic keys based on macroscopic colony characteristics and spore microscopic
330 examination (60×) (Rodriguez-Gomez et al., 2020; Melchum et al., 2023).

331

332 **2.2.6 Ice nucleation experiments**

333 The ~~ice nucleating abilities~~ INP concentration of the collected aerosol particles were
334 ~~obtained tested~~ using a UNAM-Micro-orifice Uniform Deposit Impactor-Droplet Freezing
335 Technique (UNAM-MOUDI-DFT), described in Córdoba et al. (2021) with its main features
336 shown in Fig. S3.

337

338 Aerosol particles were collected on hydrophobic glass coverslips as substrates at 0.56 µm, 1.0
339 µm, 1.8 µm, 3.2 µm, 5.6 µm and 10 µm cut-off ~~each~~ MOUDI stages (flow rate of 30.0 L min⁻¹).

340 After sampling, every substrate was stored in sealed, sterilized Petri dishes at 4 °C until its
341 analysis.

342

343 Each glass coverslip was analyzed using the UNAM-MOUDI-DFT to simulate the immersion
344 freezing mode between 0 °C and -40 °C. For the INP experiments, the glass coverslips were
345 placed on a sample holder inside the cold cell with the sample holder at the top of two blocks
346 for a sample temperature control: a heating block (copper-made block with two heating
347 resistances, 100 W and 120 V) and a cooling block (cooled by refrigerator circulator, PRO-
348 RP1090, LAUDA), with the cold block at the bottom. To induce droplet formation, humid air,
349 carried by nitrogen (grade 4.8, INFRA), is directed toward the sample holder at 0 °C. Once
350 approx. 30-40 droplets of ca. 170 µm radius are formed, and a dry airstream is introduced into
351 the cold cell to shrink the droplets, aiming to minimize contact between them. Finally, the cold
352 cell was isolated, and a temperature ramp from 0 °C to -40 °C (at a cooling rate of 10 °C min⁻¹)
353 was run until the freezing of each drop was observed. The entire process was recorded with
354 a video camera (MC500-W, JVLAB) attached to an optical microscope (Axiolab Zeiss,
355 Germany) with a 5×/0.12 magnification objective, the microscope objective being coupled to
356 the sample holder via a glass coverslip at the top of the cold cell.

357

358 From the recorded video, it is possible to determine the freezing temperature for each droplet,
359 which allows calculation of the frozen fraction (F_{ice}) and the INP number concentration as a
360 function of temperature ([INP(T)]). F_{ice} was calculated using Equation 1:

$$361 \quad F_{ice} = \frac{N_{ice}}{N_{ice} + N_{droplets}} \quad (1)$$

362 where N_{ice} and $N_{droplets}$ are the number of frozen droplets (dimensionless) and the number of
363 unfrozen droplets (dimensionless), respectively (Kanji et al., 2017).

364

365 The [INP(T)] was calculated using Equation 2 (Mason et al., 2015; Córdoba et al., 2021):

366

$$367 \quad [INP(T)] = -\ln \left(\frac{N_u(T)}{N_0} \right) \cdot \left(\frac{A_{deposit}}{A_{DFTV}} \right) \cdot N_0 \cdot f_{ne} \cdot f_{nu,0.25-0.10 \text{ mm}} \cdot f_{nu,1 \text{ mm}} \quad (2)$$

368

369 where $N_u(T)$ is the number of unfrozen droplets at T (°C), N_0 is the total number of droplets
370 (dimensionless), $A_{deposit}$ is the total area of the aerosol particles deposited on the hydrophobic
371 glass coverslip (cm²), A_{DFTV} is the area of the sample analyzed by the DFT (cm²), V is the volume
372 of air through the MOUDI (L), f_{ne} is a correction factor to account for the uncertainty associated

373 with the number of nucleation events in each experiment (dimensionless), and f_{nu} is a correction
374 factor to account for changes in particle concentration across each MOUDI sample
375 (dimensionless). Additionally, this equation accounts for the possibility that multiple particles
376 may be present within a droplet (Vali, 1996), the correction for the total area covered by
377 particles deposited on the MOUDI coverslips, and corrections for inhomogeneities in particle
378 deposition. More details of Equation 2 and the applied corrections can be found in Mason et al.
379 (2015).

380

381 **2.2.7 Data analysis**

382 The STATISTICA[®] 12 software (StatSoft, TIBCO Software Inc., USA) was employed to
383 evaluate basic statistics and cluster analysis of data from the different analysis described in
384 section 2.2. With the main objective of identifying associations among chemical species and
385 their possible sources, a cluster analysis using Ward's method of amalgamation and Pearson
386 correlation coefficients was carried out to construct dendrograms for both sampling sites.

387

388 **3. Results and Discussion**

389 **3.1 Frozen fraction and INP concentration variability**

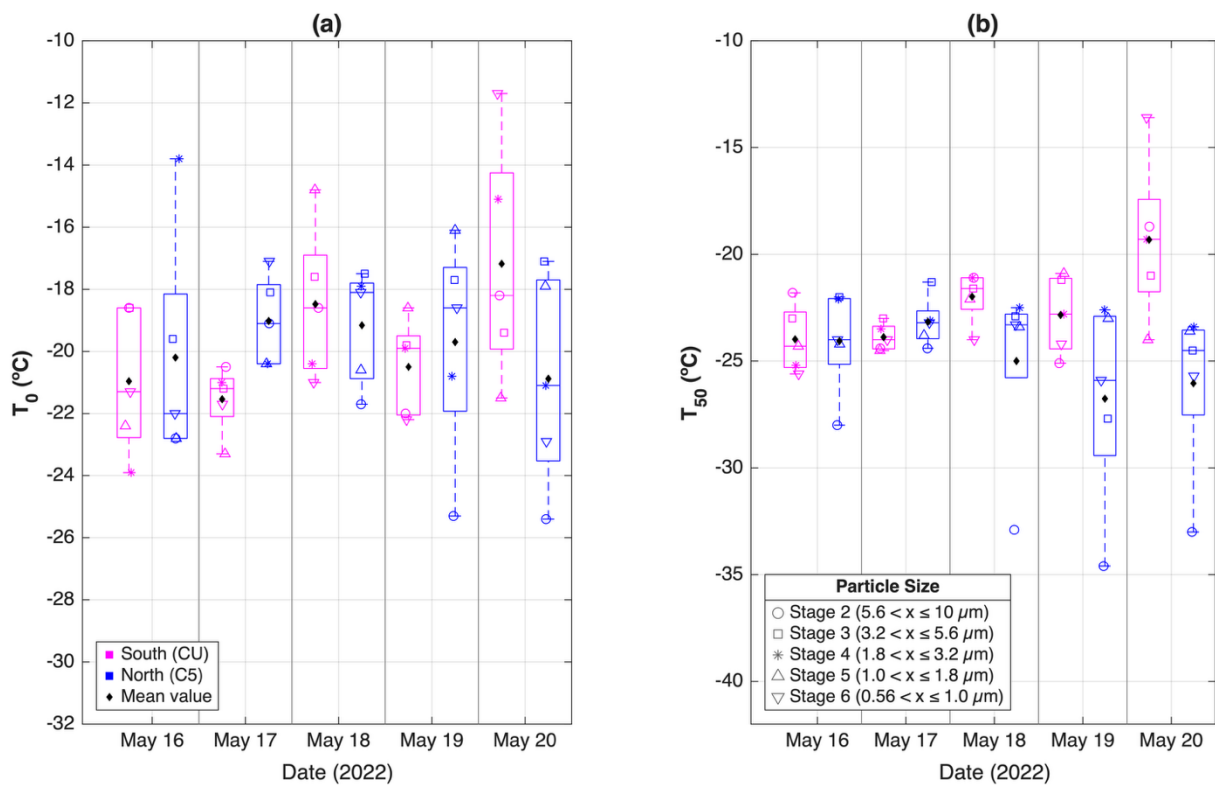
390 Following the procedure described in section 2.2.6, the frozen fraction and the INP
391 concentrations were obtained for each sample from May 16th to 20th. Figure S4 shows the frozen
392 fraction (FF) as a function of particle size (aerodynamic diameters of 4.00.56 μm to 10 μm) for
393 the northern and the southern sampling sites. This size range was selected considering that
394 super-micron particles contribute more than 70 % to the total INP population (e.g., Mason et
395 al., 2016; Córdoba et al., 2021). Aerosol particles collected in the present study were able to
396 nucleate ice at temperatures warmer than those required to freeze supercooled liquid drops (i.e.,
397 homogeneous freezing, black line). The homogeneous freezing line was determined using the
398 same procedure described in section 2.2.6 -with a brand-new substrate (i.e., without aerosol
399 particles impacted on them)-at the sample holder. The average onset freezing temperature (T_0)
400 of the homogeneous freezing experiments (i.e., -34.28 °C) is comparable with other data for
401 supercooled liquid drops such as the 100 μm (-34.15 °C) and 89 \pm 7 μm (-35.5 to -36.7 °C)
402 liquid water drops reported by Shardt et al. (2022) and Tarn et al. (2021), respectively.

403

404 For a more quantitative comparison of the ice nucleating abilities of northern and southern
405 samples, the data for the average onset freezing temperatures (T_0) and the average temperatures
406 at which 50 % of the droplets freeze (T_{50}) for each sample were calculated as were

407 ~~determined day as are~~ shown in Fig. 2. Overall, the average T_0 and T_{50} values were similar
 408 ~~between northern and southern MCMA samples.~~ The highest average T_0 difference between
 409 the northern and southern samples was registered on May 20th (Fig. 2a), with T_0 values of (~~-~~
 410 ~~204.91 ± 33.54~~) °C and (~~-~~17.23 ± 3.84) °C for C5 and CU, respectively. Additionally, the
 411 ~~greatest distinction between northern and southern T_{50} values was again recorded on May 20th,~~
 412 ~~with T_{50} = (-19.3 ± 3.8) °C on CU, and T_{50} = (-26.1 ± 3.9) °C on C5. Additionally, the highest~~
 413 ~~and lowest T_{50} values were recorded on May 20th at CU (-19.8 ± 3.6) °C and on May 19th at~~
 414 ~~C5 (-26.5 ± 4.4) °C.~~ The warmest average T_0 and T_{50} values (-17.2 °C) reported in this work
 415 ~~is are~~ slightly higher than those reported by Knopf et al. (2010) (-19.15 °C, warmer T_0 for
 416 immersion freezing mode), Rodríguez-Gómez (2021) (warmer T_0 = -19.3 °C), Cabrera-
 417 Segoviano et al. (2022) (warmer T_0 = -20.3 °C); and lower than the reported by Pereira et al.
 418 (2021) (warmer T_0 = -7.5 °C). Taking uncertainties into account, the T_0 values reported in this
 419 work partially differ from literature data for MCMA, showing a variation that local emissions
 420 could influence ~~at~~ each sampling point (e.g., Pereira et al. (2021) warmer T_0 was found at
 421 Altzomoni site, a semi-pristine area at MCMA southeast).

422



423

424 Figure 2. Boxplots of (a) Average onset freezing temperatures (T_0) and (b) average median
 425 freezing temperatures (T_{50}) for samples collected at the north (C5, blue ~~circles~~) and south (CU,
 426 magenta ~~stars~~) of Mexico City between May 16th and May 20th. The bottom and top limits of

each box represent the 25th and 75th percentiles, respectively. The horizontal line inside each box indicates the median temperature. The top and bottom whiskers show the minimum and maximum temperature values, respectively. Real values for each MOUDI stage, from 2 (larger aerodynamical size) to 6 (smaller aerodynamical size), are represented by circles, squares, asterisks, upward triangles, and downward triangles, respectively. The black diamonds indicate the mean values for each data group.

The total INP concentrations (i.e., the accumulated INP concentration, represented by the sum of each MOUDI stage INP concentration for each sample) at both sites are shown in Fig. 3a. Although the INP concentrations measured at both sites were comparable, the exemption was the May 20th sample (Fig. 3a), where higher and statistically significant differences in INP concentrations were measured in the southern site between -19^oC and -22^oC (considering the Agresti and Coull (1998) method to calculate 95 % confidence intervals). Figure 3a also indicates that the INP concentrations from the present study agree well with those reported by Cabrera-Segoviano et al. (2022) for Mexico City and by Chen et al. (2024) for Beijing (between -19^oC and -22^oC), a polluted megacity such as the MCMA.

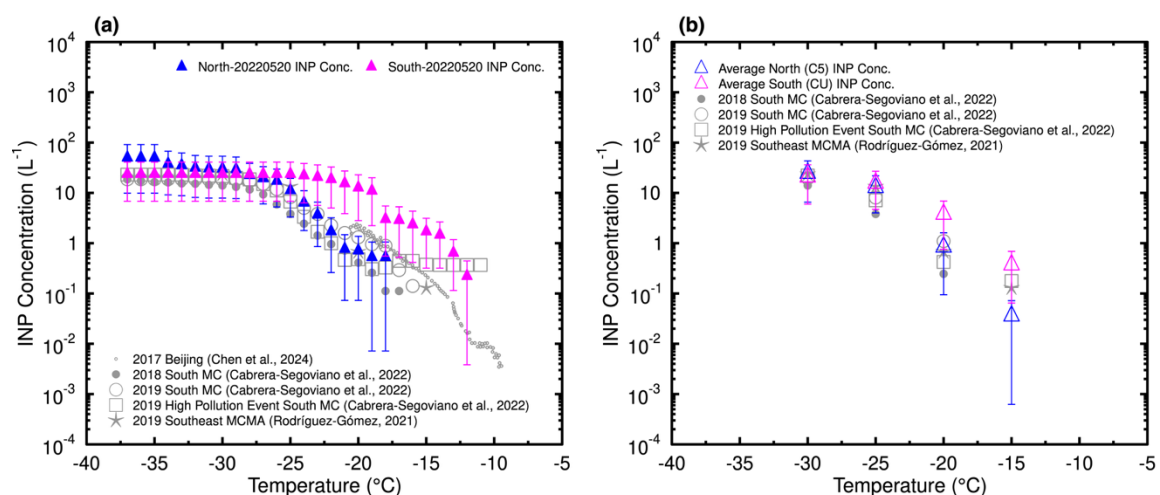


Figure 3. (a) May 16th, 17th, 18th, 19th and 20th-INP concentrations for the measurements done on May 20th, 2022 at the northern and southern site the northern and southern particles, as a function of temperature; and (b) average INP concentrations for the measurements done at the northern and southern site as a function of temperature. The colored stars and the gray dots, circles, squares, and stars represent the INP concentration values reported for Beijing (Chen et al., 2024), 2018 South Mexico City (Cabrera-Segoviano et al., 2022), 2019 South Mexico City (Cabrera-Segoviano et al., 2022), 2019 High Pollution Event at South Mexico City (Cabrera-Segoviano et al., 2022), and 2019 Southeast Mexico City Metropolitan Area (Rodríguez-

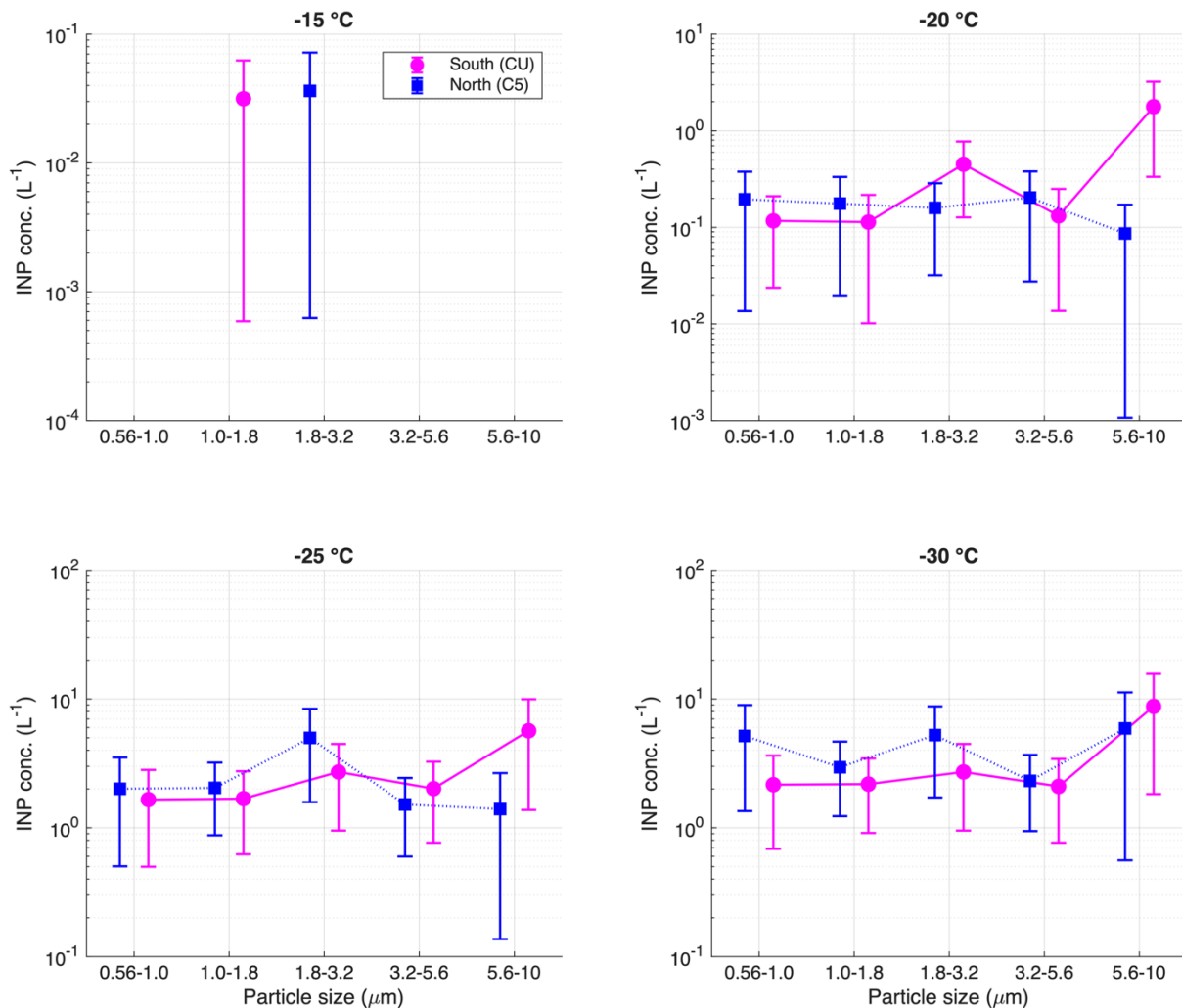
452 [Gómez, 2021](#)), respectively. [The error bars represent the carried experimental uncertainty](#)
453 [calculated using the method described by Mason et al. \(2015\)](#).

454
455 To better assess the differences in the INP concentration across the two micro-climates within
456 the MCMA, the average ~~accumulated~~-INP concentrations [\(represented by the average of all](#)
457 [samples' total INP concentration\)](#) for both sites at four different temperatures (-15 °C, -20 °C, -
458 25 °C, and -30 °C) were calculated, as shown in Fig. [3b4](#). INP concentrations at both sampling
459 sites are comparable at ~~lower all~~ temperatures (i.e., ~~-15 °C, -20 °C, -25 °C, and -30 °C~~), ~~while~~
460 ~~at higher temperatures (i.e., -20 °C and -15 °C), the southern samples are higher~~. ~~Although at~~ -
461 15 °C, a clear difference ~~of 0.34 L⁻¹~~ [close to one order of magnitude](#) can be observed between
462 both sites (C5 (0.04 ± 0.04 L⁻¹) and CU (0.38 ± 0.31 L⁻¹), ~~the difference is not statistically~~
463 ~~significant~~ (Agresti and Coull, 1998). ~~Similar to the data shown in~~ [As shown in](#) Fig. 3b, the INP
464 concentrations measured in the present study agree with ~~the concentrations~~ [those](#) reported for
465 southeastern (Rodríguez-Gómez, 2021) and southern sites (Cabrera-Segoviano et al., 2022) of
466 the MCMA.

467
468 The impact of particle size on the frozen fraction at both sampling sites does not show a clear
469 trend (Fig. S4). Likewise, Fig. [45](#) shows that the [mean](#) INP concentration [\(which represents the](#)
470 [average of all samples for each MOUDI stage\)](#) measured on ~~the~~ urban particles from the
471 MCMA is not clearly size-dependent. ~~In theory, particle size and INP efficiency are related.~~
472 This relationship is attributed to surface active sites, as larger particles contain a higher
473 concentration of active sites (Vali, 1996; Hoose and Möhler, 2012; Kanji et al., 2017); ~~however,~~
474 ~~as urban ambient samples~~ [particles](#) are a complex mixture of particles with different
475 [compositions, the relationship between particle size and INP is not straightforward as it requires](#)
476 [deeper chemical analysis to understand the heterogeneity in particles chemical composition on](#)
477 [each MOUDI stage.](#) ~~is assumption may not work on highly complex samples such as the~~
478 ~~MCMA urban particles. Different physical and chemical atmospheric processes can modify the~~
479 ~~INP surface; therefore, active sites can be deactivated in various ways through particle coating~~
480 ~~and/or aging (Cziczo et al., 2009). Thus, we hypothesize that the complexity in the~~
481 ~~physicochemical properties of urban particles, may have masked the role of particle size on~~
482 ~~their ice nucleating abilities.~~

483
484 [Even though the the discussed particle size did not show a trend, a clear difference is observed](#)
485 [at larger particle sizes \(i.e., particles between 5.6-10 μm\) between the two sampling sites. Fig.](#)

486 [2b](#) shows that four of the five samples from at least 4 of 5 stage 2 samples (i.e., particles between
 487 5.6-10 μm) from the southern site present warmer T_{50} than the same samples for the northern
 488 site. Additionally, the INP average concentrations at $-20\text{ }^\circ\text{C}$ reported in Fig. 4 shows the same
 489 behavior as shown in Fig. 4. The with a greater contribution from larger particles to the INP
 490 concentrations was found to be greater in the south of the MCMA than in the north. Although
 491 there is no chemical composition information available for these large particles size bin, the
 492 significant difference observed between the north and south sample sites suggests that a larger
 493 contribution of unknown larger urban aerosol particles could be important for heterogeneous
 494 MPC formation at the southern MCMA site. we encourage future studies to help understating
 495 the importance of PM_{10} particles. Finding a source for these large particles could help describe
 496 the southern microclimate.



497
 498 Figure 45. INP average concentration as a function of particle size at $-15\text{ }^\circ\text{C}$, $-20\text{ }^\circ\text{C}$, $-25\text{ }^\circ\text{C}$,
 499 and $-30\text{ }^\circ\text{C}$, for southern (CU, magenta) and northern (C5, blue) MCMA. The error bars
 500 represent the carried experimental uncertainty calculated using the method described by Mason
 501 et al. (2015).

502

503 **3.2 Ice nucleation activity vs. criteria pollutants and chemical composition**

504 Time series of five criteria pollutant concentrations at both sites are shown in Fig. S2. PM_{2.5}
505 concentration was found to be comparable at both sites, with a slight increase along the last part
506 of the campaign. The maximum difference in PM_{2.5} concentration between both sites was 6.60
507 $\mu\text{g m}^{-3}$. Although high hourly values of PM_{2.5} were measured (in the order of $\sim 60 \mu\text{g m}^{-3}$), they
508 cannot be considered as *high pollution episodes* as was the case described in Cabrera-Segoviano
509 et al. (2022) where PM_{2.5} concentrations above $80 \mu\text{g m}^{-3}$ were measured (Carabali et al., 2021).
510 Similar to previous studies performed within the MCMA, CO, SO₂, and NO_x concentrations
511 were higher at the northern site, with 0.6 ppm, 14 ppm, and 60 ppm maximum difference
512 between the northern and southern sites for CO, SO₂, and NO_x, respectively (Fig. S2). This
513 behavior is related to local emissions, such as gasoline-fueled vehicular emissions and industrial
514 activity (Vega et al., 2004; Castro et al., 2024).

515

516 O₃ concentrations were higher at the southern site (i.e., a 30 ppm maximum difference between
517 both sites). Local emissions from vegetation cover prevalent in southern MCMA, such as
518 volatile organic compounds (VOCs), together with local NO_x emissions and transport can
519 explain the O₃ behavior. It is well known that VOCs may participate in O₃ production by
520 photochemistry and lead to increased higher concentrations (Pinto et al., 2010; Amador-Muñoz
521 et al., 2016). Therefore, the southern site is likely enriched in biogenic secondary organic
522 aerosols (SOA) compared to the northern site (Aiken et al., 2009; Cooke et al., 2024), with
523 unknown implications in the IN-P population. Wang et al. (2012) showed that different types
524 of SOA could act as INPs via immersion freezing with potential to impact MPC formation.

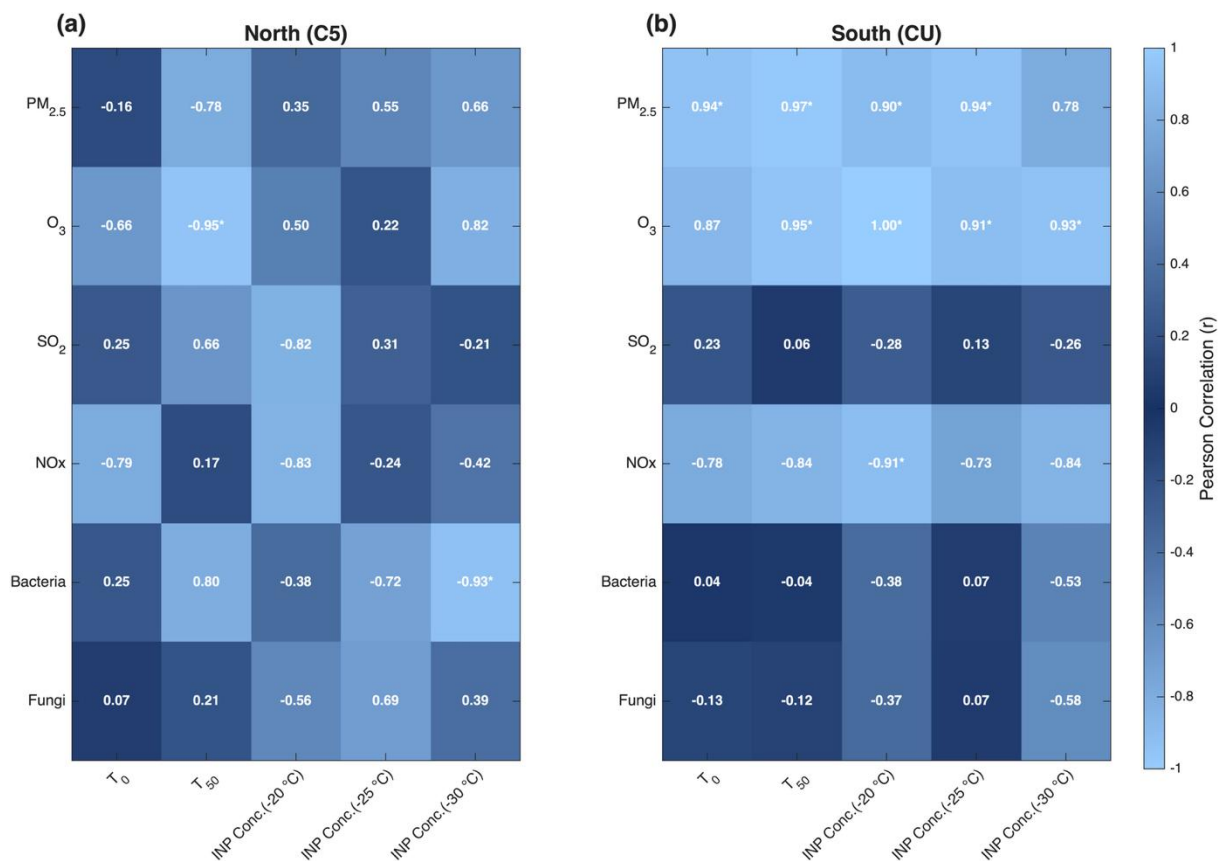
525

526 The INP concentrations shown in Figs. 3 and 4 were comparable at colder temperatures, with a
527 slightly higher concentration at the southern site observed on the last sampling day at warm
528 temperatures. Given that a slight increase in PM_{2.5} concentration was also observed on May
529 20th at the southern site (Fig. S2), there may be a small relationship between INP concentration
530 at warm temperatures and PM_{2.5}. Figure 6–5 shows the calculated Pearson determination
531 correlation coefficients between the measured criteria pollutants with T₀, T₅₀ and INP
532 concentration at -20 °C, -25 °C, and -30 °C for both sampling sites (for particles ranging
533 between 0.56 μm and 3.2 μm). Mean criteria pollutant concentrations between 08:00 h and
534 13:00 h local time were used to match the INP sampling periods. Figure- 5 shows high
535 correlations between PM_{2.5}, O₃, and the INP parameters at the southern site, implying that both

536 pollutants can impact the physicochemical properties of the INP population at this site. On the
 537 other hand, no significant correlations were found at the northern site. As the INP sizes in both
 538 sites are identical, the observed differences are likely linked with differences in the PM_{2.5}
 539 composition. As shown in Figs. 6 and S56, the PM_{2.5} elemental and ionic composition in the
 540 northern and southern sites have important differences. As the composition is clearly different,
 541 the interaction between the fine particles, and hence INPs, with O₃ is expected to differ in both
 542 sites as well. As the PM_{2.5} sampling time was much larger (24 h) than the 4 h INP sampling, a
 543 direct correlation between the elemental and ionic composition with the INP concentrations
 544 was not assessed.

545
 546 This suggest that different sources of particles could be present at both MCMA sites, but no
 547 correlation was found that anthropogenic pollution could modify INP concentration. –The
 548 relationship between PM_{2.5} and INP concentrations was has been previously evaluated (Chen
 549 et al., 2018; Bi et al., 2019; Córdoba et al., 2021; Cabrera-Segoviano et al., 2022), with highly
 550 contrasting results, but showing that urban particle concentrations alone do not affect INP
 551 concentration.

552



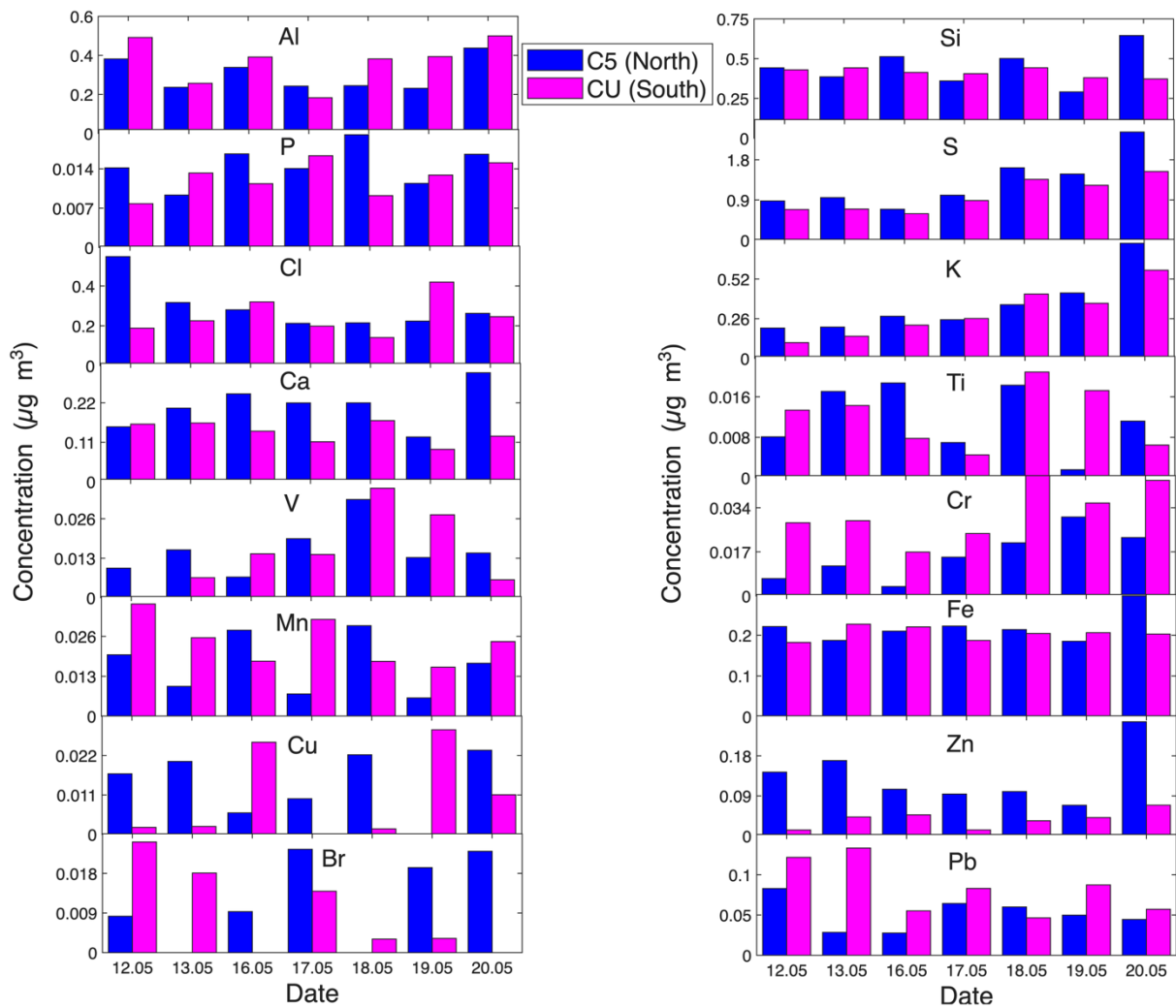
553

554 The potential relationship between the ice nucleation abilities of the analyzed urban particles

555 ~~and the other measured variables was assessed. For gaseous criteria pollutants, the southern~~
556 ~~INPs (T_0 , T_{50} , and INP Conc. at $-20\text{ }^\circ\text{C}$) positively correlated with O_3 and NO_x concentration~~
557 ~~(Fig. 6). On the other hand, the northern INPs (T_0 , T_{50} , and INP Conc. at $-20\text{ }^\circ\text{C}$) only correlated~~
558 ~~with SO_2 . Therefore, the importance of the different criteria pollutants on the ice nucleating~~
559 ~~abilities of the urban particles differs with respect to the micro-climate.~~

560
561 Figure 65. Heat map with the Pearson ~~determination~~ correlation coefficients (r) for the
562 relationships between the ~~ice nucleation abilities~~ INP parameters (i.e., T_0 , T_{50} , and INP
563 concentration at $-20\text{ }^\circ\text{C}$, $-25\text{ }^\circ\text{C}$ and $-30\text{ }^\circ\text{C}$) and the ~~composition as well as~~ ambient criteria
564 pollutants concentrations (i.e., $\text{PM}_{2.5}$, O_3 , NO_x , and SO_2) for (a) ~~southern-northern (C5U)~~ site
565 and (b) ~~northern-southern (CU5)~~ site of the MCMA. The CO concentration missing data for
566 some INP analysis sampling days explain the absence of correlations between INP parameters
567 and CO concentration. The statistically significant coefficients (with 95 % confidence level)
568 are marked with an asterisk.

569
570 The analysis of the elemental composition indicates that the concentration of 12 of the 16
571 analyzed elements (i.e., Si, P, S, Cl, K, Ca, Ti, V, Fe, Cu, Zn, and Br) was higher at the northern
572 site as shown in Fig. 67. The maximum measured concentrations were reported for Al and Si,
573 an indication of the presence of aluminum silicates from resuspended dust, as previously
574 reported (Querol et al., 2019; Córdoba et al., 2021). Pb was present at both sampling sites with
575 a maximum concentration of $0.13\text{ }\mu\text{g m}^{-3}$ and $0.08\text{ }\mu\text{g m}^{-3}$ for CU and C5, respectively. The Pb
576 sources are typically linked with local industrial activities and the usage of low quality fuels
577 (Moreno et al., 2008; Hernández-López et al., 2020). The World Health Organization (WHO)
578 recommends an annual average airborne Pb concentration of $0.5\text{ }\mu\text{g m}^{-3}$ as part of its Global
579 Air Quality Guidelines; therefore, the values reported in this work did not exceed this limit.



581

582 Figure 67. Concentration of the different individual elements analyzed by XRF on PM_{2.5} at the
 583 northern (C5, blue) and southern (CU, magenta) sites.

584

585 The maximum S concentration (i.e., 2.42 $\mu\text{g m}^{-3}$) observed in C5 is lower than the values
 586 reported in previous studies (3.24 $\mu\text{g m}^{-3}$, Castro et al., 2024; 3.38 $\mu\text{g m}^{-3}$, IMADA, 1997; 5.10
 587 $\mu\text{g m}^{-3}$, Vega et al., 2004), likely related to differences in the sampling month, but higher than
 588 the highest S concentration reported in CU (i.e., 1.54 $\mu\text{g m}^{-3}$). S and K are markers of high-
 589 pollution events in megacities, typically linked with industrial activity, gasoline combustion,
 590 and BB emissions (Ríos and Raga, 2018; Raga et al., 2021). In this study, a rise in S and K
 591 concentrations during the last sampling day (i.e., May 20th) is clearly observed and could be
 592 attributed to local and regional BB. ~~Fig-6 shows that the S and K concentrations positively~~
 593 ~~correlated with T_0 , T_{50} , and INP Conc. ($-20\text{ }^\circ\text{C}$) at the southern site. This could imply a~~
 594 ~~relationship between the INP behavior and the presence of BB particles, a relationship shown~~
 595 ~~elsewhere (-~~

596

597

598 To further explore the ~~importance of aerosol composition and its relationship with the INPs~~
599 ~~chemical composition of urban aerosol particles~~ at both sampling sites, the ion composition was
600 analyzed. Figure S565 reinforces the ~~notorious significant~~ differences in the urban particles'
601 chemical composition between the two micro-climates. The five analyzed cations (Na^+ , K^+ ,
602 Ca^{2+} , NH_4^+ , and Mg^{2+}) and the three analyzed anions (Cl^- , NO_3^- , and SO_4^{2-}) showed higher
603 concentrations at the northern site. The relationships among SO_4^{2-} , NO_3^- , and NH_4^+ at both
604 sampling sites are shown in Tables S3 and S4. The strong observed correlation suggests the
605 presence of $(\text{NH}_4)_2\text{SO}_4$ and NH_4NO_3 at both sites, two compounds produced by photochemical
606 reactions driven by ~~emissions from~~ gasoline and diesel ~~emissions~~ (Vega et al., 2004;
607 Hernández-López et al., 2020; Castro Romero et al., 2024). ~~Although the absence of~~
608 ~~Correlations between ion concentration and INP parameters are stronger at the northern site,~~
609 ~~indicating a higher the probability of photochemical products mentioned before and~~
610 ~~consequently, more probability reactions of VOCs and that lead to anthropogenic SOA cannot~~
611 ~~be discarded despised, especially at higher ozone concentrations (Hallquist et al., 2009).~~

612

613 ~~Although most of the analyzed ions showed a low correlation with the INP parameters at both~~
614 ~~sampling sites (Fig. 6), K^+ values showed strong Pearson coefficients at the southern site with~~
615 ~~T_0 , T_{50} , and INP Conc. (-20°C) values, reinforcing the influence of BB emissions on INP~~
616 ~~behavior at the southern micro-climate. Figure S676 shows that summarizes the HYSPLIT~~
617 ~~backward trajectories ran for May 2022. This, in addition the HYSPLIT backward trajectories~~
618 ~~at 250 m AGL at both MCMA sites the overlaid on the to NASA FIRMS real-time active~~
619 ~~fire locations for the sampling period (i.e., May 12th to May 20th, 2022) for May 16th to 20th~~
620 ~~showed in Fig. S7. Even though not all, backward trajectories pass through active fires~~
621 ~~locations, the overlap between some back-trajectories and active fires some punctual suggests~~
622 ~~that the besides local sources, the regional local and regional transport of BB particles could an~~
623 ~~be important for contribute to the observed differences in the the ice nucleation abilities of~~
624 ~~microclimate chemical composition, as shown elsewhere (e.g., Carabali et al., 2021)~~
625 ~~differentiation the MCMA urban particles, especially at the southern site. Additionally, Figure~~
626 ~~Fig. S676 also suggests that the air masses arriving at the northern site at noon and midnight,~~
627 ~~at 250 m and 500 m AGL, were not transported over the southern site, and vice versa show sn~~
628 ~~that air-masses in both sampling sites came from very similar directions during the sampling~~
629 ~~period, so particle transport between two sites cannot be despised at all. :~~

630

631 To evaluate potential sources of the measured urban aerosol particles, a cluster analysis was
632 applied using all the chemical species to generate a dendrogram for each sampling site.
633 Hierarchical clustering was conducted using Ward's method, with Pearson correlation
634 coefficients employed as the similarity measure. This technique groups variables by minimizing
635 increases in within-cluster variance, leading to clusters of species with similar temporal
636 patterns. The resulting dendrogram illustrates the level of similarity among variables, where
637 shorter linkage distances represent stronger relationships~~different~~. Principal cluster
638 components can be linked to a potential source as shown in previous literature analysis of
639 similar samples (Reynoso-Cruces et al., 2023). The dendrogram for the southern site (Fig.
640 S788) presents three groups: the orange cluster with anthropogenic oxidized and non-oxidized
641 species and a contribution of BB regional emissions; the ~~blue-green~~ cluster with geogenic
642 oxidized and non-oxidized species; and the ~~green-brown~~ cluster with resuspended soil
643 originated from rural areas with geogenic species and some anthropogenic contributions.
644 Likewise, the dendrogram for the northern site (Fig. S899) also shows three groups: the orange
645 cluster, which corresponds to anthropogenic oxidized and non-oxidized species; the blue
646 cluster, containing mostly anthropogenic oxidized species from fossil fuels; and the ~~green~~
647 ~~brown~~ cluster with oxidized and non-oxidized resuspended soils. This cluster analysis
648 highlights the effects of land use and BB on the chemical composition of the urban particles
649 across these two microclimates of the MCMA and denotes sample complexity. This cluster
650 analysis highlights the effect of land use and BB on the chemical composition of the urban
651 particles at these two micro-climates of the MCMA.

652

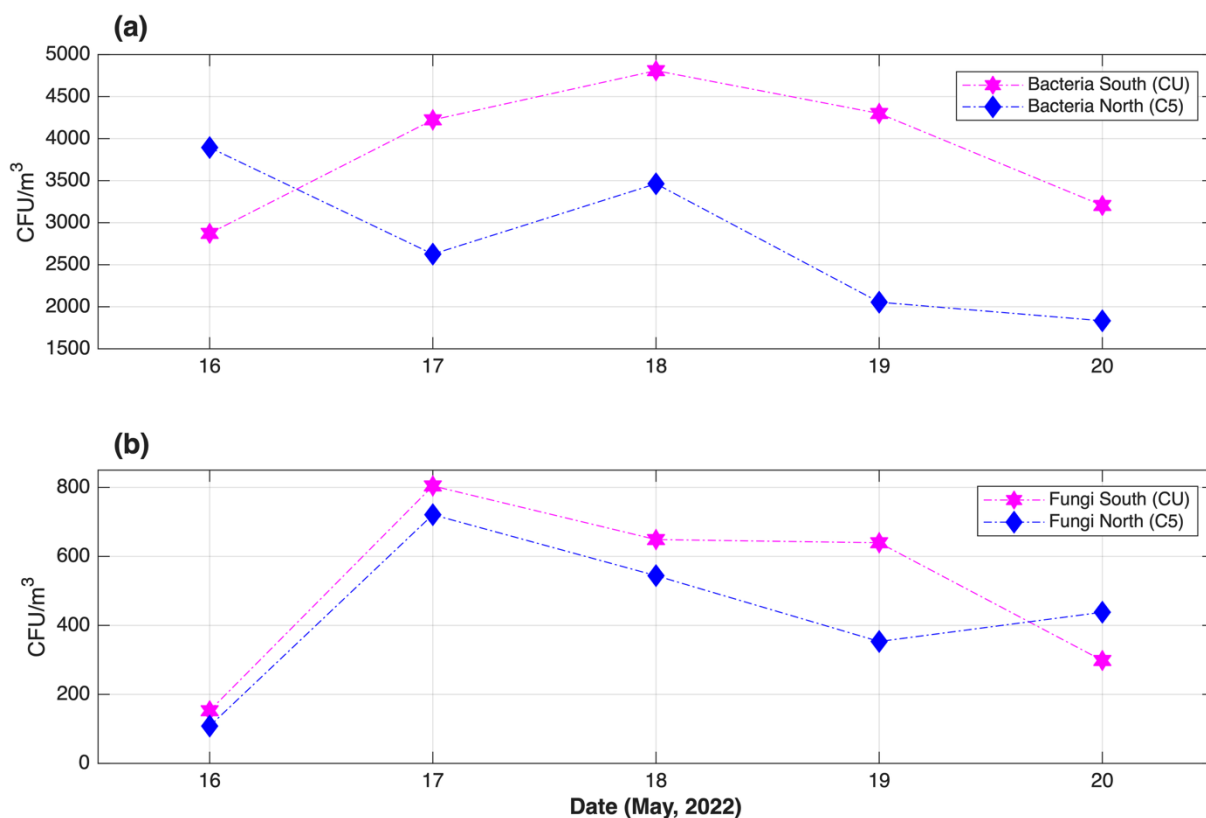
653

654 **3.3 Ice nucleation~~ing~~ activity vs. culturable microorganisms**

655 To assess the presence of biological particles at both sampling sites, the concentrations of
656 culturable bacteria and fungi were measured in parallel to the INPs. Significant daily variations
657 in bacteria and fungi concentrations at both sampling sites were observed, as shown in Fig. 78.
658 The measured CFU m⁻³ follow the same pattern at both sites, an inverse pattern with PM_{2.5}
659 concentration. The average concentrations of bacteria and fungi at the northern site were 2774
660 CFU m⁻³ and 433 CFU m⁻³, respectively; at the southern site, the average concentrations of
661 bacteria and fungi were 3882 CFU m⁻³ and 509 CFU m⁻³, respectively. The average bacteria
662 concentrations reported in this study are higher than those reported for Yucatán, México (i.e.,
663 69 CFU m⁻³) (Rodriguez-Gomez et al., 2020), Tijuana, México (i.e., 340 CFU m⁻³) (Hurtado et
664 al., 2014), northwestern Amazon, Colombia (i.e., 228 CFU m⁻³) (Russy-Velandia et al., 2025),

665 and Qingdao, China (i.e., 83 CFU m⁻³) (Li et al., 2011). In contrast, the average fungi
 666 concentrations reported in this work are lower than those reported for Yucatán, México (i.e.,
 667 1018 CFU m⁻³) (Rodriguez-Gómez et al., 2020), and are consistent with the results reported for
 668 northwestern Amazon, Colombia (i.e., 642 CFU m⁻³) (Russy-Velandia et al., 2025) and
 669 Qingdao, China (i.e., ~300 CFU m⁻³) (Li et al., 2011). Consistent with the aforementioned
 670 studies, the Gram staining analysis indicated that 57 % of the culturable bacteria were Gram-
 671 positive.

672



673

674 Figure 78. Time series of the concentration (CFU/m³) of total mesophilic a) bacteria and b)
 675 fungi measured in the northern (C5, blue) and southern (CU, magenta) sites. As comparison
 676 reference, orange markers represent the PM_{2.5} average concentration (μg m⁻³) in both sites.

677

678 A total of 21 bacterial species and eight fungal genera were identified between both sampling
 679 sites (Tables S5 and S6). Although bioparticles were clearly present at both sites, it is doubtful
 680 that they played a key role in the ice nucleating abilities of the collected urban particles as the
 681 warmest average T₀ was (-17.2 ± 3.8) °C. This is very different from the T₀ values reported for
 682 bioaerosols, typically above -10 °C (Hoose et al., 2010; Knopf et al., 2011; Wex et al., 2015;
 683 Kunert et al., 2019). Although the northern site showed positive relative higher, but not

684 ~~significant~~, correlations between ~~fungi microorganisms'~~ concentration with ~~T₅₀, INP Conc. (-~~
685 ~~20 °C), and INP Conc. (-25 °C)~~ INP parameters (Fig. 56), the low T₀ ~~and T₅₀~~-measured values,
686 ~~in comparison compared~~ to other biological INPs, indicate that the identified culturable
687 microorganisms did not play a primary role in the measured ~~ice nucleating abilities~~ INP
688 concentration of the MCMA samples. Additionally, differences between the biological and INP
689 analysis sampling methods (i.e., differences in cut-off and total sampling time) inhibits
690 quantitative correlations.

691

692 Although some of the identified bacteria and fungi genera and species have been reported to
693 act as INPs at warm temperatures (Tables S5 and S6), it is completely unknown if the MCMA
694 microorganisms contained the INA protein. Melchum et al. (2023) showed that among the 64
695 analyzed species, the most efficient INP was the *Cupriavidus pauculus* bacteria, with a T₀ and
696 T₅₀ temperatures of -11.8 °C and -17.3 °C, respectively. Therefore, as demonstrated by
697 Melchum et al. (2023) and previously by Schnell and Vali (1976), tropical biological particles
698 appear to be inefficient INPs.

699

700 The ~~variations in behavior of~~ bacterial and fungal concentration between the northern and
701 southern sites were evaluated by the ~~cross-correlations~~ Pearson correlation analysis shown in
702 Tables S7 and S8. As expected, mixed values of Pearson coefficients reflect that not all bacteria
703 and fungi found at the ~~northern-southern site~~ (closed to vegetated areas) are present in the
704 ~~southern-northern~~ site.

705

706

707 **4. Conclusions**

708 This work evaluated, for the first time, simultaneous measurements of INP abilities
709 concentration at two sites within one of the largest megacities worldwide. Aerosol particles
710 sampled in the southern and northern parts of the MCMA acted as INPs, via immersion
711 freezing, at average temperatures below $(-17.233 \pm 3.85) ^\circ\text{C}$ and $(-19.12 \pm 1.59) ^\circ\text{C}$,
712 respectively. The average INP concentrations varied between $(0.04 \pm 0.04) \text{ L}^{-1}$ and $(24.93 \pm$
713 $187) \text{ L}^{-1}$ at temperatures between $-15 ^\circ\text{C}$ and $-30 ^\circ\text{C}$. The measured INP concentrations agree
714 with those from previous studies conducted in Mexico City (Mexico) and Beijing (China),
715 showing that INP concentrations are not affected by anthropogenic emissions but are indeed
716 influenced by soil use and other local sources. Although earlier studies have shown that particle
717 size plays a role in the ~~ice nucleating abilities~~ INP concentration of Arctic, urban, marine,

718 biomass burning, and mineral dust particles (e.g., Mason et al., 2016; Córdoba et al., 2020), the
719 present results showed that the ~~ice nucleating abilities~~ INP concentration of complex urban
720 particles from the MCMA are not strongly size-dependent (see Fig. S4 and Fig. ~~46~~5).

721
722 The present results clearly demonstrated the existence of microclimates within the MCMA. The
723 INP ~~activity parameters~~ of the MCMA urban particles correlated with $PM_{2.5}$, ~~and O_3 , S, K, and~~
724 ~~K⁺, especially~~ at the southern site, corroborating that ~~the number of particle mass concentrations~~
725 ~~and particle composition~~ ozone concentration ~~are~~ very important for the southern MCMA
726 microclimate. Nevertheless, urban aerosol particles show similar INP concentrations across
727 both sites, suggesting that INP activity does not depend on a specific aerosol particulate type,
728 but rather on the bulk complex mixture of aerosol particles. ~~Also, the present results clearly~~
729 ~~demonstrated the existence of micro-climates within the MCMA.~~ Local emissions and the
730 regional transport of different particles (e.g., BB, biogenic SOA, anthropogenic SOA, mineral
731 dust particles, and bioaerosol), are highlighted as the primary sources of urban aerosol particles
732 along the MCMA. These results are consistent with previous studies in the MCMA that have
733 mostly focused on aerosol chemical composition (Molina et al., 2010; Amador-Muñoz et al.,
734 2011; Ladino et al., 2018).

735
736 Although the distance between both sampling sites is just 16 km, aerosol sources and
737 atmospheric processes linked to particle formation and aerosol aging (~~i.e., gas-to-particle~~
738 ~~conversion, organic coatings, and photochemistry~~) are quite different. This implies key local
739 implications in particle characteristics (i.e., chemical composition, particle morphology, and
740 particle size) that could impact the INP concentration. The present study demonstrates that a
741 larger contribution of unknown large urban aerosol particles (i.e., particles between 5.6-10 μm)
742 could be important for heterogeneous MPC formation at the southern MCMA site, as evidenced
743 by the rise in INP concentration at -20 °C (see Fig. 2 and Fig. 4). Therefore, if we aim to improve
744 the current understanding of aerosol-cloud interactions within this megacity, it is crucial to
745 consider the different micro-climates to avoid assuming that aerosol physicochemical and
746 biological characteristics within the megacity are homogeneous. Thus, differences in the local
747 anthropogenic activities, biogenic emissions, population density, and land use are key drivers
748 that must be considered.

749
750 Although the present work shows that air pollutants such as $PM_{2.5}$ and ozone can be linked with
751 the ice nucleating abilities of urban aerosol particles, ~~additional information and further analysis~~

752 ~~are required to fully understand the relationship between aerosol particles and cloud formation,~~
753 ~~such as particle morphology, coating, and degree of aging. it is important to understand the role~~
754 ~~and the origin of the super-micron particles as they are a large contributor to the MCMA INP~~
755 ~~population. F, more research is needed if the present results, related to mixed-phase clouds,~~
756 ~~may also apply to cirrus clouds.~~

757
758
759 **Author contributions.** KV, DR, JAC, FC, and LAL performed the field measurements. KV,
760 DR, JAC, FC, SMT, and LAL analyzed the data. GBR and LAL designed the field campaigns
761 and were responsible for funding acquisition. KV, SMT, and EN conducted the INP analysis.
762 OR supported the field campaigns and data acquisition. HA conducted the ionic composition
763 analysis. JM conducted the X-ray fluorescence chemical analysis. JAC, IR, LM, and ES
764 conducted the microorganism's identification analysis. SMT and LAL wrote the paper,
765 addressed the reviews and editing, with contributions from all coauthors.

766
767 **Competing interests.** At least one of authors is part of the Editorial board.

768
769 **Acknowledgments.** The authors thank Alison Ruiz, Maria Isabel Saavedra, Juan Carlos Pineda,
770 and Manuel García for their invaluable help. We thank Miguel Sanchez from the Mexico City
771 Atmospheric Monitoring System for sharing the criteria pollutants data and for his support in
772 using their infrastructure. We also thank the RUOA and PEMBU for sharing their
773 meteorological data. Finally, we thank the NOAA for facilitating the use of the surface maps
774 and HYSPLIT.

775
776 **Financial support.** This research was financially supported by the Consejo Nacional de
777 Humanidades, Ciencia y Tecnología (grant no. 1024827) and the Marcos Moshinsky
778 Foundation. Sebastian Mendoza-Téllez thanks SECIHTI for his PhD fellowship.

779
780 **Data availability.** Data will be made available on request.

781
782
783 **References**

784 [Agresti, A. and Coull, B. A.: Approximate is Better than “Exact” for Interval Estimation of](#)
785 [Binomial Proportions, Am. Stat., 52, 119–126,](#)
786 <https://doi.org/10.1080/00031305.1998.10480550>, 1998.

787 [Aiken, A. C., Salcedo, D., Cubison, M. J., Huffman, J. A., DeCarlo, P. F., Ulbrich, I. M.,](#)
788 [Docherty, K. S., Sueper, D., Kimmel, J. R., Worsnop, D. R., Trimborn, A., Northway, M.,](#)
789 [Stone, E. A., Schauer, J. J., Volkamer, R. M., Fortner, E., de Foy, B., Wang, J., Laskin, A.,](#)
790 [Shutthanandan, V., Zheng, J., Zhang, R., Gaffney, J., Marley, N. A., Paredes-Miranda, G.,](#)
791 [Arnott, W. P., Molina, L. T., Sosa, G., and Jimenez, J. L.: Mexico City aerosol analysis during](#)
792 [MILAGRO using high resolution aerosol mass spectrometry at the urban supersite \(T0\) – Part](#)
793 [1: Fine particle composition and organic source apportionment, Atmos Chem Phys,](#)
794 <https://doi.org/10.5194/acp-9-6633-2009>, 2009.

795 [Aldape, F., Flores M., J., Diaz, R. V., Morales, J. R., Cahill, T. A., and Saravia, L.: Seasonal](#)
796 [study of the composition of atmospheric aerosols in Mexico City, Int. J. PIXE, 01, 355–371,](#)
797 <https://doi.org/10.1142/S012908359100024X>, 1991.

798 [Amador-Muñoz, O., Villalobos-Pietrini, R., Miranda, J., and Vera-Avila, L. E.: Organic](#)
799 [compounds of PM_{2.5} in Mexico Valley: Spatial and temporal patterns, behavior and sources,](#)
800 [Sci. Total Environ., 409, 1453–1465, https://doi.org/10.1016/j.scitotenv.2010.11.026](#), 2011.

801 [Amador-Muñoz, O., Bazán-Torija, S., Villa-Ferreira, S. A., Villalobos-Pietrini, R., Bravo-](#)
802 [Cabrera, J. L., Munive-Colín, Z., Hernández-Mena, L., Saldarriaga-Noreña, H., and Murillo-](#)
803 [Tovar, M. A.: Opposing seasonal trends for polycyclic aromatic hydrocarbons and PM₁₀:](#)
804 [Health risk and sources in southwest Mexico City, Atmospheric Res., 122, 199–212,](#)
805 <https://doi.org/10.1016/j.atmosres.2012.10.003>, 2013.

806 [Amador-Muñoz, O., Misztal, P. K., Weber, R., Worton, D. R., Zhang, H., Drozd, G., and](#)
807 [Goldstein, A. H.: Sensitive detection of *n*-alkanes using a mixed ionization mode proton-](#)
808 [transfer-reaction mass spectrometer, Atmospheric Meas. Tech., 9, 5315–5329,](#)
809 <https://doi.org/10.5194/amt-9-5315-2016>, 2016.

810 [Behzadi, F., Wasti, A., Haque Rahat, S., Tracy, J. N., and Ray, P. A.: Analysis of the climate](#)
811 [change signal in Mexico City given disagreeing data sources and scattered projections, J.](#)
812 [Hydrol. Reg. Stud., 27, 100662, https://doi.org/10.1016/j.ejrh.2019.100662](#), 2020.

813 [Bi, K., McMeeking, G. R., Ding, D. P., Levin, E. J. T., DeMott, P. J., Zhao, D. L., Wang, F.,](#)
814 [Liu, Q., Tian, P., Ma, X. C., Chen, Y. B., Huang, M. Y., Zhang, H. L., Gordon, T. D., and Chen,](#)
815 [P.: Measurements of Ice Nucleating Particles in Beijing, China, J. Geophys. Res. Atmospheres,](#)
816 [124, 8065–8075, https://doi.org/10.1029/2019JD030609](#), 2019.

817 [Burrows, S. M., McCluskey, C. S., Cornwell, G., Steinke, I., Zhang, K., Zhao, B., Zawadowicz,](#)
818 [M., Raman, A., Kulkarni, G., China, S., Zelenyuk, A., and DeMott, P. J.: Ice-Nucleating](#)
819 [Particles That Impact Clouds and Climate: Observational and Modeling Research Needs, Rev.](#)
820 [Geophys., 60, e2021RG000745, https://doi.org/10.1029/2021RG000745](#), 2022.

821 [Cabrera-Segoviano, D., Pereira, D. L., Rodriguez, C., Raga, G. B., Miranda, J., Alvarez-Ospina,](#)
822 [H., and Ladino, L. A.: Inter-annual variability of ice nucleating particles in Mexico City, Atmos.](#)
823 [Environ., 273, 118964, https://doi.org/10.1016/j.atmosenv.2022.118964](#), 2022.

824 [Carabali, G., Villanueva-Macias, J., Ladino, L. A., Álvarez-Ospina, H., Raga, G. B., Andraca-](#)
825 [Ayala, G., Miranda, J., Grutter, M., Silva, Ma. M., and Riveros-Rosas, D.: Characterization of](#)

826 [aerosol particles during a high pollution episode over Mexico City, *Sci. Rep.*, 11, 22533,](#)
827 <https://doi.org/10.1038/s41598-021-01873-4>, 2021.

828 [Castro Romero, T., Peralta, O., Prieto, C., Santiago, N., Alvarez-Ospina, H., García Martínez,](#)
829 [R., Saavedra Rosado, I., Espinosa Fuentes, M. D. L. L., Hernández, E., Miranda, J., Gómez, V.,](#)
830 [Solís, C., Salcedo, D., Torres-Jardón, R., Martínez-Arroyo, A., Ortíz Álvarez, A., Ruíz-](#)
831 [Suárez, G., and Ortiz, E.: Characterization of PM_{2.5} during ACU15 campaign in Mexico City,](#)
832 [Geofísica Int.](#), 63, 1225–1238, <https://doi.org/10.22201/igeof.2954436xe.2024.63.4.1745>,
833 [2024.](#)

834 [Celada-Murillo, A.-T., Carreón-Sierra, S., Salcido, A., Castro, T., Peralta, O., and Georgiadis,](#)
835 [T.: Main Characteristics of Mexico City Local Wind Events during the MILAGRO 2006](#)
836 [Campaign within a Meso- \$\beta\$ Scale Lattice Wind Modeling Approach, *ISRN Meteorol.*, 2013,](#)
837 [1–14, https://doi.org/10.1155/2013/605210](#), 2013.

838 [Chen, J., Wu, Z., Augustin-Bauditz, S., Grawe, S., Hartmann, M., Pei, X., Liu, Z., Ji, D., and](#)
839 [Wex, H.: Ice-nucleating particle concentrations unaffected by urban air pollution in Beijing,](#)
840 [China, *Atmospheric Chem. Phys.*, 18, 3523–3539, https://doi.org/10.5194/acp-18-3523-2018,](#)
841 [2018.](#)

842 [Chen, J., Wu, Z., Gong, X., Qiu, Y., Chen, S., Zeng, L., and Hu, M.: Anthropogenic Dust as a](#)
843 [Significant Source of Ice-Nucleating Particles in the Urban Environment, *Earths Future*, 12,](#)
844 [e2023EF003738, https://doi.org/10.1029/2023EF003738](#), 2024.

845 [Cooke, M. E., Waters, C. M., Asare, J. Y., Mirrieles, J. A., Holen, A. L., Frauenheim, M. P.,](#)
846 [Zhang, Z., Gold, A., Pratt, K. A., Surratt, J. D., Ladino, L. A., and Ault, A. P.: Atmospheric](#)
847 [Aerosol Sulfur Distribution and Speciation in Mexico City: Sulfate, Organosulfates, and](#)
848 [Isoprene-Derived Secondary Organic Aerosol from Low NO Pathways, *ACS EST Air*, 1, 1037–](#)
849 [1052, https://doi.org/10.1021/acsestair.4c00048](#), 2024.

850 [Córdoba, F., Ramírez-Romero, C., Cabrera, D., Raga, G. B., Miranda, J., Alvarez-Ospina, H.,](#)
851 [Rosas, D., Figueroa, B., Kim, J. S., Yakobi-Hancock, J., Amador, T., Gutierrez, W., García,](#)
852 [M., Bertram, A. K., Baumgardner, D., and Ladino, L. A.: Measurement report: Ice nucleating](#)
853 [abilities of biomass burning, African dust, and sea spray aerosol particles over the Yucatán](#)
854 [Peninsula, *Atmospheric Chem. Phys.*, 21, 4453–4470, https://doi.org/10.5194/acp-21-4453-](#)
855 [2021](#), 2021.

856 [Doran, J. C., Arnott, W. P., Barnard, J. C., Cary, R., Coulter, R., Fast, J. D., Kassianov, E. I.,](#)
857 [Kleinman, L., Laulainen, N. S., Martin, T., Paredes-Miranda, G., Pekour, M. S., Shaw, W. J.,](#)
858 [Smith, D. F., and Springston, S. R.: The T1-T2 study: evolution of aerosol properties downwind](#)
859 [of Mexico City, *Atmospheric Chem. Phys. Discuss.*, 6 \(6\), 12967-12999.,](#)
860 <https://doi.org/10.5194/acp-7-1585-2007>, 2007.

861 [Draxler, R.R., R., G. D.: HYSPLIT \(HYbrid Single-Particle Lagrangian Integrated Trajectory\)](#)
862 [Model, 2010.](#)

863 [Edgerton, S. A., Bian, X., Doran, J. C., Fast, J. D., Hubbe, J. M., Malone, E. L., Shaw, W. J.,](#)
864 [Whiteman, C. D., Zhong, S., Arriaga, J. L., Ortiz, E., Ruiz, M., Sosa, G., Vega, E., Limon, T.,](#)
865 [Guzman, F., Archuleta, J., Bossert, J. E., Elliot, S. M., Lee, J. T., McNair, L. A., Chow, J. C.,](#)
866 [Watson, J. G., Coulter, R. L., Doskey, P. V., Gaffney, J. S., Marley, N. A., Neff, W., and Petty,](#)

867 [R.: Particulate Air Pollution in Mexico City: A Collaborative Research Project, J. Air Waste](#)
868 [Manag. Assoc., 49, 1221–1229, <https://doi.org/10.1080/10473289.1999.10463915>, 1999.](#)

869 [Espinosa, A., Miranda, J., and Pineda, J.C: Uncertainty evaluation in correlated quantities:](#)
870 [application to elemental analysis of atmospheric aerosols, Rev. Mex. Física, 56 \(1\), 134–140,](#)
871 [2010.](#)

872 [Espinosa, A. A., Reyes-Herrera, J., Miranda, J., Mercado, F., Veytia, M. A., Cuautle, M., and](#)
873 [Cruz, J. I.: Development of an X-ray fluorescence spectrometer for environmental science](#)
874 [applications, Instrum. Sci. Technol., 40, 603–617,](#)
875 [https://doi.org/10.1080/10739149.2012.693560, 2012.](#)

876 [Gimeno, L., Sorí, R., Vázquez, M., Stojanovic, M., Algarra, I., Eiras-Barca, J., Gimeno-Sotelo,](#)
877 [L., and Nieto, R.: Extreme precipitation events, WIREs Water, 9, e1611,](#)
878 [https://doi.org/10.1002/wat2.1611, 2022.](#)

879 [Hasenkopf, C. A., Veghte, D. P., Schill, G. P., Lodoysamba, S., Freedman, M. A., and Tolbert,](#)
880 [M. A.: Ice nucleation, shape, and composition of aerosol particles in one of the most polluted](#)
881 [cities in the world: Ulaanbaatar, Mongolia, Atmos. Environ., 139, 222–229,](#)
882 [https://doi.org/10.1016/j.atmosenv.2016.05.037, 2016.](#)

883 [Hernández-López, A. E., Miranda Martín Del Campo, J., Mugica-Álvarez, V., Hernández-](#)
884 [Valle, B. L., Mejía-Ponce, L. V., Pineda-Santamaría, J. C., Reynoso-Cruces, S., Mendoza-](#)
885 [Flores, J. A., and Rozanes-Valenzuela, D.: A study of PM_{2.5} elemental composition in](#)
886 [southwest Mexico City and development of receptor models with positive matrix factorization,](#)
887 [Rev. Int. Contam. Ambient., <https://doi.org/10.20937/RICA.54066>, 2020.](#)

888 [Hernández-López, A. E., Santos-Medina, G. L., Morton-Bermea, O., Hernández-Álvarez, E.,](#)
889 [Villalobos-Pietrini, R., and Amador-Muñoz, O.: Chemical speciation of organic compounds](#)
890 [and elemental compositions of PM_{2.5} in Mexico City: Spatial-seasonal distribution, emission](#)
891 [sources, and formation processes, Atmospheric Res., 292, 106868,](#)
892 [https://doi.org/10.1016/j.atmosres.2023.106868, 2023.](#)

893 [Heymsfield, A. J., Schmitt, C., Chen, C.-C.-J., Bansemer, A., Gettelman, A., Field, P. R., and](#)
894 [Liu, C.: Contributions of the Liquid and Ice Phases to Global Surface Precipitation:](#)
895 [Observations and Global Climate Modeling, J. Atmospheric Sci., 77, 2629–2648,](#)
896 [https://doi.org/10.1175/JAS-D-19-0352.1, 2020.](#)

897 [Hoose, C. and Möhler, O.: Heterogeneous ice nucleation on atmospheric aerosols: a review of](#)
898 [results from laboratory experiments, Atmospheric Chem. Phys., 12, 9817–9854,](#)
899 [https://doi.org/10.5194/acp-12-9817-2012, 2012.](#)

900 [Hoose, C., Kristjánsson, J. E., and Burrows, S. M.: How important is biological ice nucleation](#)
901 [in clouds on a global scale?, Environ. Res. Lett., 5, 024009, \[9326/5/2/024009, 2010.\]\(https://doi.org/10.1088/1748-
902 <a href=\)](#)

903 [Houze, R. A.: Cloud dynamics, Second edition., Academic Press, Oxford, England, 2014.](#)

904 [Hurtado, L., Rodríguez, G., López, J., Castillo, J. E., Molina, L., Zavala, M., and Quintana, P.](#)
905 [J. E.: Characterization of atmospheric bioaerosols at 9 sites in Tijuana, Mexico, Atmos.](#)
906 [Environ., 96, 430–436, <https://doi.org/10.1016/j.atmosenv.2014.07.018>, 2014.](#)

907 [Población: https://www.inegi.org.mx/temas/estructura/](https://www.inegi.org.mx/temas/estructura/), last access: 10 October 2025.

908 [Jahl, L. G., Brubaker, T. A., Polen, M. J., Jahn, L. G., Cain, K. P., Bowers, B. B., Fahy, W. D.,](#)
909 [Graves, S., and Sullivan, R. C.: Atmospheric aging enhances the ice nucleation ability of](#)
910 [biomass-burning aerosol, *Sci. Adv.*, 7, <https://doi.org/10.1126/sciadv.abd3440>, 2021.](#)

911 [Jahn, L. G., Polen, M. J., Jahl, L. G., Brubaker, T. A., Somers, J., and Sullivan, R. C.: Biomass](#)
912 [combustion produces ice-active minerals in biomass-burning aerosol and bottom ash, *Proc.*](#)
913 [Natl. Acad. Sci., 117, 21928–21937, <https://doi.org/10.1073/pnas.1922128117>, 2020.](#)

914 [Jáuregui, E.: El clima de la Ciudad de México, 1. ed., Instituto de Geografía, UNAM: Plaza y](#)
915 [Valdés Editores, México, D.F, 131 pp., 2000.](#)

916 [Kanji, Z. A., Ladino, L. A., Wex, H., Boose, Y., Burkert-Kohn, M., Cziczo, D. J., and Krämer,](#)
917 [M.: Overview of Ice Nucleating Particles, *Meteorol. Monogr.*, 58, 1.1-1.33,](#)
918 <https://doi.org/10.1175/AMSMONOGRAPHS-D-16-0006.1>, 2017.

919 [Knopf, D. A., Wang, B., Laskin, A., Moffet, R. C., and Gilles, M. K.: Heterogeneous nucleation](#)
920 [of ice on anthropogenic organic particles collected in Mexico City, *Geophys. Res. Lett.*, 37,](#)
921 [2010GL043362, <https://doi.org/10.1029/2010GL043362>, 2010.](https://doi.org/10.1029/2010GL043362)

922 [Knopf, D. A., Alpert, P. A., Wang, B., and Aller, J. Y.: Stimulation of ice nucleation by marine](#)
923 [diatoms, *Nat. Geosci.*, 4, 88–90, <https://doi.org/10.1038/ngeo1037>, 2011.](#)

924 [Kunert, A. T., Pöhlker, M. L., Tang, K., Krevert, C. S., Wieder, C., Speth, K. R., Hanson, L.](#)
925 [E., Morris, C. E., Schmale Iii, D. G., Pöschl, U., and Fröhlich-Nowoisky, J.: Macromolecular](#)
926 [fungal ice nuclei in *Fusarium*: effects of physical and chemical processing, *Biogeosciences*,](#)
927 [16, 4647–4659, <https://doi.org/10.5194/bg-16-4647-2019>, 2019.](https://doi.org/10.5194/bg-16-4647-2019)

928 [Ladino, L. A., Raga, G. B., and Baumgardner, D.: On particle-bound polycyclic aromatic](#)
929 [hydrocarbons \(PPAH\) and links to gaseous emissions in Mexico City, *Atmos. Environ.*, 194,](#)
930 [31–40, <https://doi.org/10.1016/j.atmosenv.2018.09.022>, 2018.](https://doi.org/10.1016/j.atmosenv.2018.09.022)

931 [Lezama, J. L. and Vargas, V. I.: Las fuerzas rectoras de la contaminación del aire en la Ciudad](#)
932 [de México, MIT Integr. Program Urban Reg. Glob. Air Pollut. Rep. NO8 Camb. MA, 2000.](#)

933 [Li, C., Zwiers, F., Zhang, X., Chen, G., Lu, J., Li, G., Norris, J., Tan, Y., Sun, Y., and Liu,](#)
934 [M.: Larger Increases in More Extreme Local Precipitation Events as Climate Warms,](#)
935 [Geophys. Res. Lett., 46, 6885–6891, <https://doi.org/10.1029/2019GL082908>, 2019.](https://doi.org/10.1029/2019GL082908)

936 [Li, M., Qi, J., Zhang, H., Huang, S., Li, L., and Gao, D.: Concentration and size distribution of](#)
937 [bioaerosols in an outdoor environment in the Qingdao coastal region, *Sci. Total Environ.*, 409,](#)
938 [3812–3819, <https://doi.org/10.1016/j.scitotenv.2011.06.001>, 2011.](https://doi.org/10.1016/j.scitotenv.2011.06.001)

939 [Mason, R. H., Chou, C., McCluskey, C. S., Levin, E. J. T., Schiller, C. L., Hill, T. C. J.,](#)
940 [Huffman, J. A., DeMott, P. J., and Bertram, A. K.: The micro-orifice uniform deposit impactor–](#)
941 [droplet freezing technique \(MOUDI-DFT\) for measuring concentrations of ice nucleating](#)
942 [particles as a function of size: improvements and initial validation, *Atmospheric Meas. Tech.*,](#)
943 [8, 2449–2462, <https://doi.org/10.5194/amt-8-2449-2015>, 2015.](https://doi.org/10.5194/amt-8-2449-2015)

944 [Mason, R. H., Si, M., Chou, C., Irish, V. E., Dickie, R., Elizondo, P., Wong, R., Brintnell, M.,](#)
945 [Elsasser, M., Lassar, W. M., Pierce, K. M., Leaitch, W. R., MacDonald, A. M., Platt, A., Toom-](#)

946 [Sauntry, D., Sarda-Estève, R., Schiller, C. L., Suski, K. J., Hill, T. C. J., Abbatt, J. P. D.,](#)
947 [Huffman, J. A., DeMott, P. J., and Bertram, A. K.: Size-resolved measurements of ice-](#)
948 [nucleating particles at six locations in North America and one in Europe, *Atmospheric Chem.*](#)
949 [Phys., 16, 1637–1651, <https://doi.org/10.5194/acp-16-1637-2016>, 2016.](#)

950 [Melchum, A., Córdoba, F., Salinas, E., Martínez, L., Campos, G., Rosas, I., Garcia-Mendoza,](#)
951 [E., Olivos-Ortiz, A., Raga, G. B., Pizano, B., Silva, Ma. M., and Ladino, L. A.: Maritime and](#)
952 [continental microorganisms collected in Mexico: An investigation of their ice-nucleating](#)
953 [abilities, *Atmospheric Res.*, 293, 106893, <https://doi.org/10.1016/j.atmosres.2023.106893>,](#)
954 [2023.](#)

955 [Met Office, 2023, "Microclimates," National Meteorological Library and Archive Factsheet 14,](#)
956 [https://www.metoffice.gov.uk/binaries/content/assets/metofficegovuk/pdf/research/library-](#)
957 [and-archive/library/publications/factsheets/factsheet_14-microclimates_2023.pdf, last access:](#)
958 [17 February 2026.](#)

959 [Molina, H., Yang, Y., Ruch, T., Kim, J.-W., Mortensen, P., Otto, T., Nalli, A., Tang, Q.-Q.,](#)
960 [Lane, M. D., Chaerkady, R., and Pandey, A.: Temporal Profiling of the Adipocyte Proteome](#)
961 [during Differentiation Using a Five-Plex SILAC Based Strategy, *J. Proteome Res.*, 8, 48–58,](#)
962 [https://doi.org/10.1021/pr800650r, 2009.](#)

963 [Molina, L. T., Madronich, S., Gaffney, J. S., Apel, E., De Foy, B., Fast, J., Ferrare, R., Herndon,](#)
964 [S., Jimenez, J. L., Lamb, B., Osornio-Vargas, A. R., Russell, P., Schauer, J. J., Stevens, P. S.,](#)
965 [Volkamer, R., and Zavala, M.: An overview of the MILAGRO 2006 Campaign: Mexico City](#)
966 [emissions and their transport and transformation, *Atmospheric Chem. Phys.*, 10, 8697–8760,](#)
967 [https://doi.org/10.5194/acp-10-8697-2010, 2010.](#)

968 [Molina, M. J. and Molina, L. T.: Megacities and Atmospheric Pollution, *J. Air Waste Manag.*](#)
969 [Assoc., 54, 644–680, <https://doi.org/10.1080/10473289.2004.10470936>, 2004.](#)

970 [Moreno, T., Querol, X., Pey, J., Minguillón, M. C., Pérez, N., Alastuey, A., Bernabé, R. M.,](#)
971 [Blanco, S., Cárdenas, B., Eichinger, W., Salcido, A., and Gibbons, W.: Spatial and temporal](#)
972 [variations in inhalable CuZnPb aerosols within the Mexico City pollution plume, *J. Environ.*](#)
973 [Monit., 10, 370, <https://doi.org/10.1039/b716507b>, 2008.](#)

974 [Mülmenstädt, J., Sourdeval, O., Delanoë, J., and Quaas, J.: Frequency of occurrence of rain](#)
975 [from liquid-, mixed-, and ice-phase clouds derived from A-Train satellite retrievals, *Geophys.*](#)
976 [Res. Lett., 42, 6502–6509, <https://doi.org/10.1002/2015GL064604>, 2015.](#)

977 [Ohneiser, K., Seifert, P., Schimmel, W., Senf, F., Gaudek, T., Radenz, M., Teisseire, A.,](#)
978 [Ettrichrätz, V., Vogl, T., Mahernndl, N., Pfeifer, N., Henneberger, J., Miller, A. J., Omanovic,](#)
979 [N., Fuchs, C., Zhang, H., Ramelli, F., Spirig, R., Kötsche, A., Kalesse-Los, H., Maahn, M.,](#)
980 [Corden, H., Berne, A., Hajipour, M., Griesche, H., Hofer, J., Engelmann, R., Skupin, A.,](#)
981 [Ansmann, A., and Baars, H.: Impact of seeder-feeder cloud interaction on precipitation](#)
982 [formation: a case study based on extensive remote-sensing, in situ and model data, *Atmospheric*](#)
983 [Chem. Phys., 25, 17363–17386, <https://doi.org/10.5194/acp-25-17363-2025>, 2025.](#)

984 [Pereira, D. L., Silva, Ma. M., García, R., Raga, G. B., Alvarez-Ospina, H., Carabali, G., Rosas,](#)
985 [I., Martinez, L., Salinas, E., Hidalgo-Bonilla, S., and Ladino, L. A.: Characterization of ice](#)
986 [nucleating particles in rainwater, cloud water, and aerosol samples at two different tropical](#)

latitudes, *Atmospheric Res.*, 250, 105356, <https://doi.org/10.1016/j.atmosres.2020.105356>, 2021.

Pinto, D. M., Blande, J. D., Souza, S. R., Nerg, A.-M., and Holopainen, J. K.: Plant Volatile Organic Compounds (VOCs) in Ozone (O₃) Polluted Atmospheres: The Ecological Effects, *J. Chem. Ecol.*, 36, 22–34, <https://doi.org/10.1007/s10886-009-9732-3>, 2010.

Prenni, A. J., DeMott, P. J., Sullivan, A. P., Sullivan, R. C., Kreidenweis, S. M., and Rogers, D. C.: Biomass burning as a potential source for atmospheric ice nuclei: Western wildfires and prescribed burns, *Geophys. Res. Lett.*, 39, <https://doi.org/10.1029/2012gl051915>, 2012.

Purdy, J. C., Austin, G. L., Seed, A. W., and Cluckie, I. D.: Radar evidence of orographic enhancement due to the seeder feeder mechanism, *Meteorol. Appl.*, 12, 199–206, <https://doi.org/10.1017/S1350482705001672>, 2005.

Querol, X., Pey, J., Minguillón, M. C., Pérez, N., Alastuey, A., Viana, M., Moreno, T., Bernabé, R. M., Blanco, S., Cárdenas, B., Vega, E., Sosa, G., Escalona, S., Ruiz, H., and Artíñano, B.: PM speciation and sources in Mexico during the MILAGRO-2006 Campaign, *Atmospheric Chem. Phys.*, 8, 111–128, <https://doi.org/10.5194/acp-8-111-2008>, 2008.

Querol, X., Tobías, A., Pérez, N., Karanasiou, A., Amato, F., Stafoggia, M., Pérez García-Pando, C., Ginoux, P., Forastiere, F., Gumy, S., Mudu, P., and Alastuey, A.: Monitoring the impact of desert dust outbreaks for air quality for health studies, *Environ. Int.*, 130, 104867, <https://doi.org/10.1016/j.envint.2019.05.061>, 2019.

Raga, G. B., Ladino, L. A., Baumgardner, D., Ramirez-Romero, C., Córdoba, F., Alvarez-Ospina, H., Rosas, D., Amador, T., Miranda, J., Rosas, I., Jaramillo, A., Yakobi-Hancock, J., Kim, J. S., Martínez, L., Salinas, E., and Figueroa, B.: ADABBOY: African Dust And Biomass Burning Over Yucatan, *Bull. Am. Meteorol. Soc.*, 102, E1543–E1556, <https://doi.org/10.1175/BAMS-D-20-0172.1>, 2021.

Reynoso-Cruces, S., Miranda-Martín-Del-Campo, J., and Pineda-Santamaría, J. C.: Elemental composition of PM₁₀ in indoor environments of a scientific research institution and risk assessment, *Environ. Pollut. Bioavailab.*, 35, 2232108, <https://doi.org/10.1080/26395940.2023.2232108>, 2023.

Riojas-Rodríguez, H., Álamo-Hernández, U., Texcalac-Sangrador, J. L., and Romieu, I.: Health impact assessment of decreases in PM₁₀ and ozone concentrations in the Mexico City Metropolitan Area. A basis for a new air quality management program, *Salud Pública México*, 56, 579, <https://doi.org/10.21149/spm.v56i6.7384>, 2014.

Ríos, B. and Raga, G. B.: Spatio-temporal distribution of burned areas by ecoregions in Mexico and Central America, *Int. J. Remote Sens.*, 39, 949–970, <https://doi.org/10.1080/01431161.2017.1392641>, 2018.

Rodríguez-Gómez, C.: Variabilidad de los núcleos de glaciación en la capa límite y la tropósfera libre en Altzomoni, y su influencia en la formación de nubes mixtas, Universidad Nacional Autónoma de México, México, CDMX, 128 pp., 2021.

Rodriguez-Gomez, C., Ramirez-Romero, C., Cordoba, F., Raga, G. B., Salinas, E., Martinez, L., Rosas, I., Quintana, E. T., Maldonado, L. A., Rosas, D., Amador, T., Alvarez, H., and Ladino, L. A.: Characterization of culturable airborne microorganisms in the Yucatan

1028 [Peninsula, Atmos. Environ., 223, 117183, https://doi.org/10.1016/j.atmosenv.2019.117183,](https://doi.org/10.1016/j.atmosenv.2019.117183)
1029 [2020.](https://doi.org/10.1016/j.atmosenv.2019.117183)

1030 [Rogers, R. R. and Yau, M. K.: A short course in cloud physics, Third edition., Butterworth-](https://doi.org/10.1016/j.atmosenv.2019.117183)
1031 [Heinemann, Burlington, Massachusetts, 1 pp., 1996.](https://doi.org/10.1016/j.atmosenv.2019.117183)

1032 [Rosas, D., Silva, M. M., Figueroa, B., Morton-Bermea, O., Miranda, J., Alvarez, H., Puig, T.](https://doi.org/10.1016/j.atmosenv.2019.117183)
1033 [P., Morales, J., Uuh, J., Hernández-Alvarez, E., Novelo, S., Olivares, J., Salcedo, D., Rosas, I.,](https://doi.org/10.1016/j.atmosenv.2019.117183)
1034 [Ponce, C., Raga, G. B., and Ladino, L. A.: African dust particles over the western Caribbean:](https://doi.org/10.1016/j.atmosenv.2019.117183)
1035 [Chemical characterization, Atmos. Environ., 347, 121095,](https://doi.org/10.1016/j.atmosenv.2019.117183)
1036 [https://doi.org/10.1016/j.atmosenv.2025.121095, 2025.](https://doi.org/10.1016/j.atmosenv.2019.117183)

1037 [Russy-Velandia, L., Ramírez, O., Barrera, J., Mendoza-Téllez, S., Álvarez, H., Patiño, M. C.,](https://doi.org/10.1016/j.atmosenv.2019.117183)
1038 [and Ladino, L. A.: Approach to culturable bioaerosols and their environmental drivers at a](https://doi.org/10.1016/j.atmosenv.2019.117183)
1039 [border site in the northwestern Amazon, Atmospheric Environ. X, 27, 100362,](https://doi.org/10.1016/j.atmosenv.2019.117183)
1040 [https://doi.org/10.1016/j.aeaoa.2025.100362, 2025.](https://doi.org/10.1016/j.atmosenv.2019.117183)

1041 [Salcido, A., Carreón-Sierra, S., Georgiadis, T., Celada-Murillo, A.-T., and Castro, T.: Lattice](https://doi.org/10.1016/j.atmosenv.2019.117183)
1042 [Wind Description and Characterization of Mexico City Local Wind Events in the 2001–2006](https://doi.org/10.1016/j.atmosenv.2019.117183)
1043 [Period, Climate, 3, 542–562, https://doi.org/10.3390/cli3030542, 2015.](https://doi.org/10.1016/j.atmosenv.2019.117183)

1044 [Schnell, R. C. and Vali, G.: Biogenic Ice Nuclei: Part I. Terrestrial and Marine Sources, J.](https://doi.org/10.1016/j.atmosenv.2019.117183)
1045 [Atmospheric Sci., 33, 1554–1564, https://doi.org/10.1175/1520-](https://doi.org/10.1016/j.atmosenv.2019.117183)
1046 [0469\(1976\)033%253C1554:BINPIT%253E2.0.CO;2, 1976.](https://doi.org/10.1016/j.atmosenv.2019.117183)

1047 [Shardt, N., Isenrich, F. N., Waser, B., Marcolli, C., Kanji, Z. A., deMello, A. J., and Lohmann,](https://doi.org/10.1016/j.atmosenv.2019.117183)
1048 [U.: Homogeneous freezing of water droplets for different volumes and cooling rates, Phys.](https://doi.org/10.1016/j.atmosenv.2019.117183)
1049 [Chem. Chem. Phys., 24, 28213–28221, https://doi.org/10.1039/D2CP03896J, 2022.](https://doi.org/10.1016/j.atmosenv.2019.117183)

1050 [Tabari, H.: Climate change impact on flood and extreme precipitation increases with water](https://doi.org/10.1016/j.atmosenv.2019.117183)
1051 [availability, Sci. Rep., 10, 13768, https://doi.org/10.1038/s41598-020-70816-2, 2020.](https://doi.org/10.1016/j.atmosenv.2019.117183)

1052 [Tarn, M. D., Sikora, S. N. F., Porter, G. C. E., Shim, J., and Murray, B. J.: Homogeneous](https://doi.org/10.1016/j.atmosenv.2019.117183)
1053 [Freezing of Water Using Microfluidics, Micromachines, 12, 223,](https://doi.org/10.1016/j.atmosenv.2019.117183)
1054 [https://doi.org/10.3390/mi12020223, 2021.](https://doi.org/10.1016/j.atmosenv.2019.117183)

1055 [Toll, V., Rahu, J., Keernik, H., Trofimov, H., Voormansik, T., Manshausen, P., Hung, E.,](https://doi.org/10.1016/j.atmosenv.2019.117183)
1056 [Michelson, D., Christensen, M. W., Post, P., Junninen, H., Murray, B. J., Lohmann, U., Watson-](https://doi.org/10.1016/j.atmosenv.2019.117183)
1057 [Parris, D., Stier, P., Donaldson, N., Storelvmo, T., Kulmala, M., and Bellouin, N.: Glaciation](https://doi.org/10.1016/j.atmosenv.2019.117183)
1058 [of liquid clouds, snowfall, and reduced cloud cover at industrial aerosol hot spots, Science, 386,](https://doi.org/10.1016/j.atmosenv.2019.117183)
1059 [756–762, https://doi.org/10.1126/science.adl0303, 2024.](https://doi.org/10.1016/j.atmosenv.2019.117183)

1060 [Trofimov, H., Post, P., Gryspeerdt, E., and Toll, V.: Meteorological Conditions Favorable for](https://doi.org/10.1016/j.atmosenv.2019.117183)
1061 [Strong Anthropogenic Aerosol Impacts on Clouds, J. Geophys. Res. Atmospheres, 127,](https://doi.org/10.1016/j.atmosenv.2019.117183)
1062 [e2021JD035871, https://doi.org/10.1029/2021JD035871, 2022.](https://doi.org/10.1016/j.atmosenv.2019.117183)

1063 [Vali, G.: Ice Nucleation — a review, in: Nucleation and Atmospheric Aerosols 1996, Elsevier,](https://doi.org/10.1016/j.atmosenv.2019.117183)
1064 [271–279, https://doi.org/10.1016/B978-008042030-1/50066-4, 1996.](https://doi.org/10.1016/j.atmosenv.2019.117183)

1065 [Vega, E., Reyes, E., Ruiz, H., García, J., Sánchez, G., Martínez-Villa, G., González, U., Chow,](https://doi.org/10.1016/j.atmosenv.2019.117183)
1066 [J. C., and Watson, J. G.: Analysis of PM_{2.5} and PM₁₀ in the Atmosphere of Mexico City during](https://doi.org/10.1016/j.atmosenv.2019.117183)

1067 [2000-2002, J. Air Waste Manag. Assoc., 54, 786–798,](#)
1068 <https://doi.org/10.1080/10473289.2004.10470952>, 2004.

1069 [Wex, H., Augustin-Bauditz, S., Boose, Y., Budke, C., Curtius, J., Diehl, K., Dreyer, A., Frank,](#)
1070 [F., Hartmann, S., Hiranuma, N., Jantsch, E., Kanji, Z. A., Kiselev, A., Koop, T., Möhler, O.,](#)
1071 [Niedermeier, D., Nillius, B., Rösch, M., Rose, D., Schmidt, C., Steinke, I., and Stratmann, F.:](#)
1072 [Intercomparing different devices for the investigation of ice nucleating particles using Snomax[®]](#)
1073 [as test substance, Atmospheric Chem. Phys., 15, 1463–1485, https://doi.org/10.5194/acp-15-](#)
1074 [1463-2015, 2015.](#)

1075 [Zhao, B., Wang, Y., Gu, Y., Liou, K.-N., Jiang, J. H., Fan, J., Liu, X., Huang, L., and Yung, Y.](#)
1076 [L.: Ice nucleation by aerosols from anthropogenic pollution, Nat. Geosci., 12, 602–607,](#)
1077 <https://doi.org/10.1038/s41561-019-0389-4>, 2019.

1078 [Zhu, Z., Peng, C., Li, X., Zhang, R., Dai, X., Jiang, B., and Chen, J.: Remote Sensing-Based](#)
1079 [Analysis of Precipitation Events: Spatiotemporal Characterization across China, Water, 16,](#)
1080 [2345, https://doi.org/10.3390/w16162345, 2024.](#)

1081